

Citation: Tollis S, Singh J, Palou R, Thattikota Y, Ghazal G, Coulombe-Huntington J, et al. (2022) The microprotein Nrs1 rewires the G1/S transcriptional machinery during nitrogen limitation in budding yeast. PLoS Biol 20(3): e3001548. https://doi.org/10.1371/journal.pbio.3001548

Academic Editor: Sophie G. Martin, University of Lausanne, SWITZERLAND

Received: December 21, 2020
Accepted: January 19, 2022
Published: March 3, 2022

Peer Review History: PLOS recognizes the benefits of transparency in the peer review process; therefore, we enable the publication of all of the content of peer review and author responses alongside final, published articles. The editorial history of this article is available here: https://doi.org/10.1371/journal.pbio.3001548

Copyright: © 2022 Tollis et al. This is an open access article distributed under the terms of the Creative Commons Attribution License, which permits unrestricted use, distribution, and reproduction in any medium, provided the original author and source are credited.

Data Availability Statement: Supplemental text and figures are provided in the supplemental text file <u>S1 Text</u> and <u>S1–S7</u> Figs. Supplemental tables 1 to 6 are provided as <u>S1–S6</u> Tables. Raw gels

RESEARCH ARTICLE

The microprotein Nrs1 rewires the G1/S transcriptional machinery during nitrogen limitation in budding yeast

Sylvain Tollis ^{1,2} *, Jaspal Singh ³ *, Roger Palou^{2†}, Yogitha Thattikota^{2‡}, Ghada Ghazal², Jasmin Coulombe-Huntington², Xiaojing Tang³, Susan Moore ², Deborah Blake ², Eric Bonneil ², Catherine A. Royer⁴, Pierre Thibault², Mike Tyers²*

- 1 Institute of Biomedicine, University of Eastern Finland, Kuopio, Finland, 2 Institute for Research in Immunology and Cancer, University of Montréal, Montréal, Québec, Canada, 3 Lunenfeld-Tanenbaum Research Institute, Mount Sinai Hospital, Toronto, Ontario, Canada, 4 Department of Biological Sciences, Rensselaer Polytechnic Institute, Troy, New York, United States of America
- These authors contributed equally to this work.
- Eurrent address: Montreal Neurological Institute, McGill University, Montréal, Quebec, Canada; Department of Neurology and Neurosurgery, McGill University, Montreal, Quebec, Canada ‡ RP and YT also contributed equally to this work.
- * sylvain.tollis@uef.fi (ST); md.tyers@umontreal.ca (MT)

Abstract

Commitment to cell division at the end of G1 phase, termed Start in the budding yeast *Saccharomyces cerevisiae*, is strongly influenced by nutrient availability. To identify new dominant activators of Start that might operate under different nutrient conditions, we screened a genome-wide ORF overexpression library for genes that bypass a Start arrest caused by absence of the G1 cyclin Cln3 and the transcriptional activator Bck2. We recovered a hypothetical gene *YLR053c*, renamed *NRS1* for Nitrogen-Responsive Start regulator 1, which encodes a poorly characterized 108 amino acid microprotein. Endogenous Nrs1 was nuclear-localized, restricted to poor nitrogen conditions, induced upon TORC1 inhibition, and cell cycle-regulated with a peak at Start. *NRS1* interacted genetically with *SWI4* and *SWI6*, which encode subunits of the main G1/S transcription factor complex SBF. Correspondingly, Nrs1 physically interacted with Swi4 and Swi6 and was localized to G1/S promoter DNA. Nrs1 exhibited inherent transactivation activity, and fusion of Nrs1 to the SBF inhibitor Whi5 was sufficient to suppress other Start defects. Nrs1 appears to be a recently evolved microprotein that rewires the G1/S transcriptional machinery under poor nitrogen conditions.

Introduction

All organisms have evolved adaptive regulatory mechanisms to optimize fitness in the face of ever-changing environmental conditions. This ability to adapt is particularly important for unicellular organisms, which lack the capacity to establish the internal homeostatic environments of metazoan species. In the budding yeast *Saccharomyces cerevisiae*, different carbon

images are provided in the supplemental file S1 Raw Images. Raw quantitative data are provided in the supplemental files <u>S1-S7</u> Data as indicated in the text. The mass spectrometry data have been deposited to the ProteomeXchange Consortium via the PRIDE [Perez-Riverol Y, Csordas A, Bai J, Bernal-Llinares M, Hewapathirana S, Kundu DJ, et al. The PRIDE database and related tools and resources in 2019: improving support for quantification data. Nucleic Acids Res. 2019;47 (D1):D442-D50] partner repository with the dataset identifier PXD018681 and DOI 10.6019/ PXD018681. The RNA-sequencing data have been deposited to the Gene Expression Omnibus database (GEO, NCBI, accession number GSE179366).

Funding: This work was supported by a grant from the Canadian Institutes of Health Research (FDN-167277) to M.T. (https://cihr-irsc.gc.ca/), a Genomics Technology Platform award from Genome Canada to M.T. and P.T. (https://www. genomecanada.ca), a Natural Sciences and Engineering Research Council grant (NSERC 311598) to P.T. (https://www.nserc-crsng.gc.ca/), a Genomics Applications Partnership Program award from Genome Canada and Genome Quebec to P.T. (https://www.genomeguebec.com/, https:// www.genomecanada.ca/), a National Science Foundation grant (PHYS 1806638) to C.A.R. (https://www.nsf.gov/), an Institute for Data Valorisation (IVADO, https://ivado.ca/) postdoctoral fellowship to J.C.-H., a Canada Research Chair in Systems and Synthetic Biology to M. T. (https:// www.chairs-chaires.gc.ca/), and a Sigrid Jusélius Foundation grant to S.T. (https://www. sigridjuselius.fi/). The funders had no role in study design, data collection and analysis, decision to publish, or preparation of the manuscript.

Competing interests: The authors have declared that no competing interests exist.

Abbreviations: ChIP, chromatin immunoprecipitation; CTD, carboxyl-terminal domain; FDR, false discovery rate; FOV, field of view; MBF, MCB-Binding Factor; MHC, major histocompatibility complex; MS—MS, tandem MS; NRS1, Nitrogen-Responsive Start regulator 1; PKA, protein kinase A; PTM, posttranslational modification; RICS, raster image correlation spectroscopy; Ribi, ribosome biogenesis; RNA-seq, RNA sequencing; RP, ribosomal protein; SBF, SCB-Binding Factor; SEP, small ORF-encoded peptide; SGA, synthetic genetic array; sN&B, scanning Number and Brightness; TOR, target of rapamycin; WT, wild-type; YNB+Pro, YNB + 0.4% proline + 2% glucose.

and nitrogen sources can dramatically affect the rates of cell growth and division, as well as developmental programs [1]. Yeast cells commit to division at the end of G1 phase, an event referred to as Start [2,3]. In order to pass Start, cells must achieve a characteristic critical size threshold that dynamically adjusts to changing nutrient availability, thereby optimizing competitive fitness [3]. How nutrient conditions modulate the growth and division machinery at the molecular level is still largely unknown.

Start initiates a complex G1/S transcriptional program of approximately 200 genes that encode proteins necessary for bud emergence, DNA replication, spindle pole body duplication, and other processes. This program is controlled by 2 transcription factor complexes, SBF (Swi4/6 Cell Cycle Box [SCB]-binding factor) and MBF (MluI Cell Cycle Box [MCB]-binding factor), each comprised of related DNA-binding proteins, Swi4 and Mbp1, respectively, coupled to a common regulatory subunit Swi6 [4,5]. Individually Swi4 and Mbp1 are not essential, but a double $swi4\Delta mbp1\Delta$ mutant is inviable [6], consistent with the significant overlap between SBF and MBF binding sites in G1/S promoters [7–10]. In pre-Start cells that have not achieved critical cell size, SBF is inhibited by the Whi5 transcriptional repressor [11-13]. At Start, the G1 cyclin (Cln)-Cdc28 protein kinases phosphorylate both SBF and Whi5 to disrupt the SBF-Whi5 interaction and trigger Whi5 nuclear export [12-14]. The upstream G1 cyclin Cln3 is thought to initiate a positive feedback loop in which SBF-dependent expression of CLN1/2 further amplifies Cln-Cdc28 activity and thus SBF activation [15,16]. The expression of Cln3 itself does not rely on SBF-dependent positive feedback [17]. Although CLN3 was isolated as a potent dose-dependent activator of Start [18,19], the size-dependent mechanism whereby Cln3-Cdc28 initiates the SBF positive feedback loop remains uncertain [20–28]. CLN3 is essential only in the absence of other parallel activators of Start, most notably BCK2, which encodes a general transcriptional activator [29,30].

Connections between the main yeast nutrient signaling conduits, the cell size threshold, and Start have been established. Activation of the protein kinase A (PKA) pathway by glucose represses CLN1 and other G1/S transcripts, which may increase the cell size threshold in rich nutrients [31,32]. The TOR signaling network, which controls many aspects of cell growth including the rate of ribosome biogenesis (Ribi), has been linked to the size threshold [11,33–35]. The TORC1 complex phosphorylates and activates the effector kinase Sch9 and the master transcription factor Sfp1 to activate ribosomal protein (RP) and Ribi genes [33,34,36]. Deletion of either SFP1 or SCH9 abrogates the carbon source–dependent control of cell size [33]. The Rim15 kinase, which is active under respiratory growth conditions in poor carbon sources, suppresses the Cdc55 phosphatase that dephosphorylates Whi5 and thereby contributes to Whi5 inactivation even when Cln3 activity is low [37]. Poor nutrient conditions also increase the expression of the G1/S transcription factors and thereby activate Start at a smaller cell size [22]. Notably, though, a $cln3\Delta bck2\Delta whi5\Delta$ triple mutant is completely viable and still responds to nutrient cues, suggesting that nutrient regulation of Start may be partly independent of the Cln3-Bck2-Whi5-SBF axis [12,33].

To identify activators of Start that might act in parallel to the central Cln3-Bck2-Whi5 pathway, we screened for dosage suppressors of the lethal $cln3\Delta$ $bck2\Delta$ Start arrest phenotype [12,13,38,39]. The screen identified YLR053c, a poorly characterized hypothetical gene that encodes a recently evolved 108 amino acid microprotein, which we renamed NRS1 for Nitrogen-Responsive Start regulator 1. Nrs1 was only expressed in poor nitrogen conditions and was cell cycle regulated with peak nuclear localization at Start. Nrs1 interacted genetically and physically with SBF and caused a small size phenotype when overexpressed in wild-type cells. Nrs1 exhibited intrinsic transactivation activity and direct fusion of Nrs1 to Whi5 was sufficient to reduce cell size in rich carbon sources and rescue the $cln3\Delta$ $bck2\Delta$ lethality. These

results demonstrate that the recently evolved Nrs1 microprotein allows cells to adapt to poor nitrogen conditions by rewiring the Start transcriptional machinery.

Results

A genome-wide screen identifies overexpression of YLR053c as a rescue of $cln3\Delta \ bck2\Delta$ lethality

We constructed a $cln3\Delta$ $bck2\Delta$ whi5::GAL1-WHI5 strain that is viable in glucose but not galactose medium due to conditional WHI5 expression [12,13]. We used synthetic genetic array (SGA) methodology to cross this query strain to an array of 5,280 strains that each of contained a GAL1-GST-ORF 2- μ m high copy plasmid [40–42] and assessed the growth of the resulting array on galactose medium (Fig 1A and 1B). Three replicates of the screen identified 12 genes that reproducibly rescued the $cln3\Delta$ $bck2\Delta$ lethal Start arrest (S1 Table). These genes included the G1 cyclins CLN1 and CLN3 but not other known Start activators such as CLN2, BCK2, SWI4, and SWI6, possibly due to the high level of WHI5 expression used in our screen, and/or overexpression toxicity of particular genes. We recovered 10 genes not known to be Start regulators. Notably, the short hypothetical ORF YLR053c restored $cln3\Delta$ $bck2\Delta$ growth to the same extent as CLN3, as validated by direct transformation of the query strain with GAL1-YLR053c and GAL1-CLN3 constructs (Fig 1C). Other prospective high copy rescue genes, such as YEA4 (Fig 1C), could not be confirmed by direct transformation.

YLR053c encodes a 108 residue microprotein that is only poorly characterized. Microproteins are often encoded by newly evolved proto-genes that are thought to form a genetic reservoir that fuels adaptive evolution [43]. To gain insight into YLR053c locus evolution, we aligned the Ylr053c protein sequence from S. cerevisiae with predicted orthologs from other yeast species (Fig 1D and 1E). To estimate the extent to which YLR053c locus evolved across these species, we used the standard dN/dS metric that measures the ratio of single DNA site substitution rates at nonsynonymous codons (dN) versus synonymous codons (dS). The YLR053c locus appears to have evolved relatively rapidly within the Saccharomyces sensu stricto group, with a dN/dS ratio in the 98th, 79th, and 90th percentile in Saccharomyces mikatae, Saccharomyces bayanus, and Saccharomyces castellii, respectively, as compared with S. cerevisiae (see S1A Fig). In comparison, the evolution of other core Start regulators was closer to the genome median, with dN/dS ratios in the 74th, 77th, and 58th percentile for WHI5, 69th, 75th, and 31st percentile for SWI4, and 82nd, 51st, and 43rd percentile for SWI6. A 17 amino acid sequence at the Ylr053c carboxyl-terminal region was conserved even in more distant yeasts such as Kluyveromyces waltii (Fig 1E). Given its genetic role at Start and expression pattern (see below), we renamed the YLR053c gene NRS1 for Nitrogen-Responsive Start regulator 1.

Nrs1 is induced by rapamycin and nitrogen limitation

To understand the function of Nrs1, we first sought to characterize its endogenous expression at the protein level. We performed scanning Number and Brightness (sN&B) confocal microscopy to localize and quantify an Nrs1-GFPmut3 fusion protein at the subcellular scale in live wild-type cells under a range of conditions [22,44]. GFPmut3, a monomeric fast-folding GFP mutant [45], will be referred to here as GFP for brevity. Nrs1-GFP was not detected in cells grown on either SC + 2% glucose or SC + 2% raffinose medium (Fig 2A), consistent with previous analysis of *YLR053/NRS1* mRNA levels [46]. In contrast, Nrs1-GFP was readily detected in the nucleus of cells grown overnight to mid log-phase in nitrogen-limited (YNB + 0.4% proline + 2% glucose, abbreviated YNB+Pro) medium (Fig 2A), also in accord with published genome-wide transcriptome analyses under various nutrient

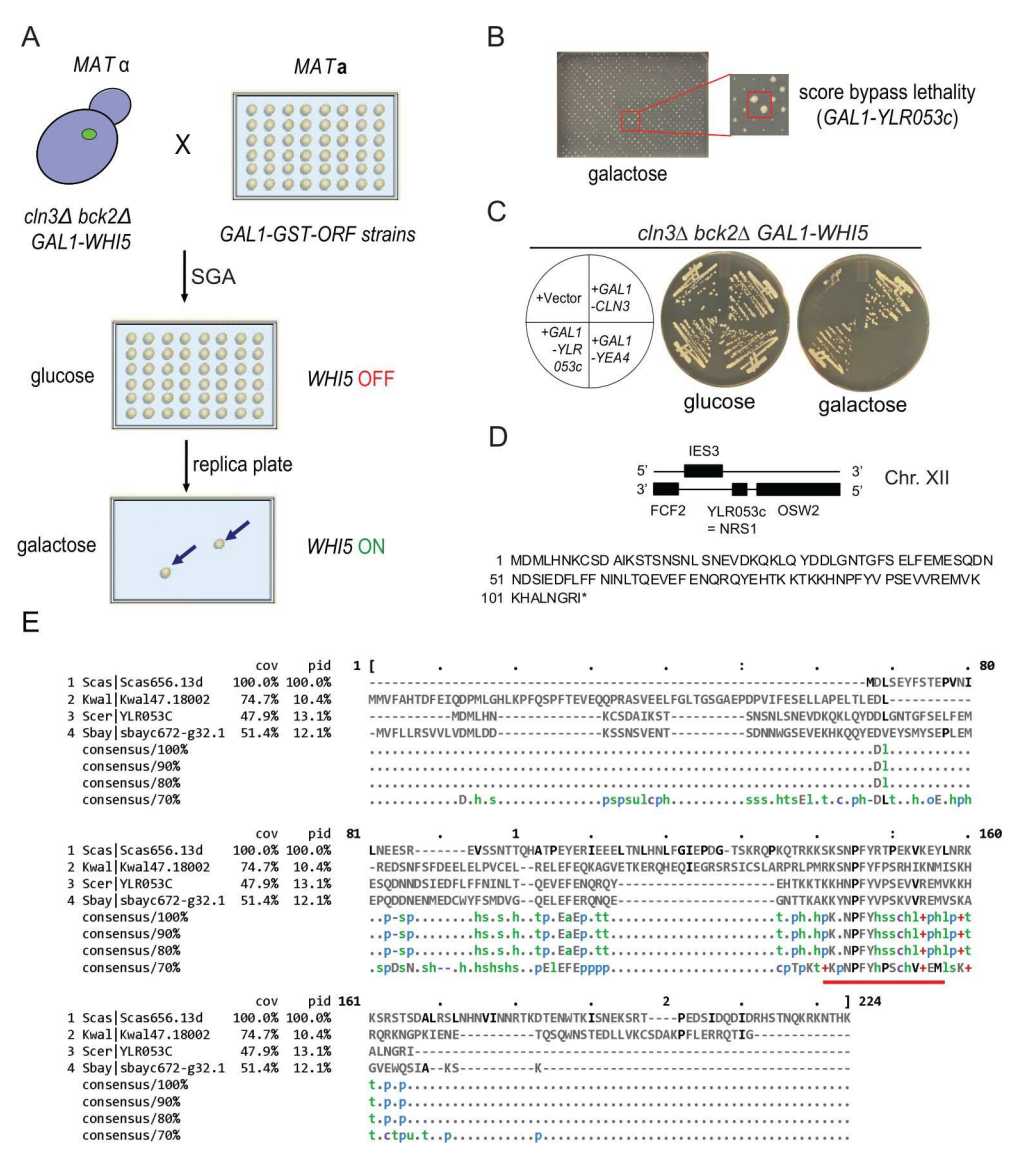


Fig 1. A genome-wide screen identifies YLR053c/NRS1 as a dosage suppressor of cln3Δ bck2Δ lethality. (A) Schematic of SGA genetic screen for dosage suppressors of cln3Δ bck2Δ lethality. (B) Representative screen plate scored for growth on galactose medium. Red box, GAL1-YLR053c. (C) Comparison of growth at 30°C for the indicated strains streaked onto either glucose or galactose medium. YEA4 was a candidate hit that did not validate. (D) Chromosomal region around YLR053c/NRS1 on Chr. XII and translated 108 amino acid (12.7 kDa) protein sequence. (E) Ylr053c/Nrs1 protein sequence in S. cerevisiae (top) aligned with sequences of other yeast species. Conservation of a KKXNPFYVPSXVVREMV motif at the carboxyl terminus is indicated by a red bar. NRS1, Nitrogen-Responsive Start regulator 1; SGA, synthetic genetic array.

https://doi.org/10.1371/journal.pbio.3001548.g001

conditions [47] and the presence of binding sites for the Gln3 transcription factor in the *NRS1* promoter [48,49]. Induction of Nrs1 upon the switch to nitrogen-limited YNB+Pro medium required a long incubation time, as Nrs1-GFP signal above autofluorescence background could not be detected after 7 hours in YNB+Pro but was clearly visible after 22 hours growth to mid-log phase in YNB+Pro (S1B Fig). Inhibition of TORC1 with 100 nM rapamycin induced Nrs1-GFP expression and nuclear localization within 1 hour in rich SC + 2% glucose medium (Fig 2A), as also evident by immunoblot analysis of an endogenously tagged Nrs1 $^{13\text{MYC}}$ strain treated with rapamycin (S1C Fig). These expression patterns were

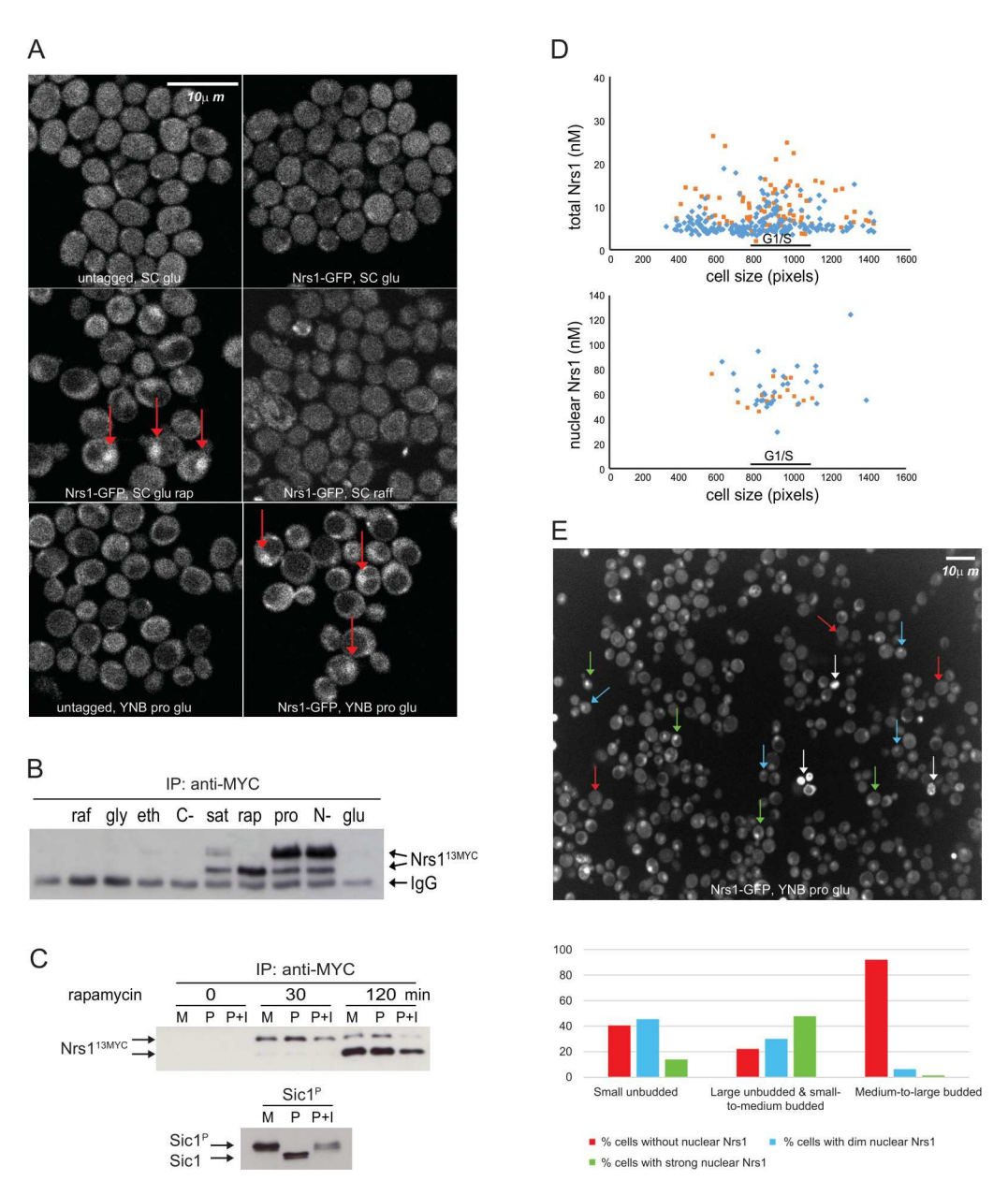


Fig 2. Nitrogen limitation and rapamycin treatment induce cell cycle-regulated Nrs1 expression. (A) sN&B images of untagged and NRS1-GFP strains. Cells were grown and imaged in SC + 2% glucose with or without 100 nM rapamycin, SC + 2% raffinose or nitrogen-limited medium (YNB +0.4% proline + 2% glucose + His, Leu, Met, Ura; labeled YNB+Pro), as indicated. Scale bar is 10 µm. The same intensity scale was used for all conditions. (B) Abundance of Nrs1^{13MYC} in various nutrient conditions as determined by immunoblot of anti-MYC immune complexes. raf, 2% raffinose; gly, 2% glycerol; eth, 2% ethanol; C-, no carbon source; sat, saturated culture; rap, 100 nM rapamycin; pro, 0.4% proline; N-, no nitrogen source; glu, 2% glucose. IgG indicates antibody light chain. A raw image of the original immunoblot is provided in S1 Raw Images. (C) Nrs1 MYC immunoprecipitates from a rapamycin treatment time course were either mock-treated (M, negative control), treated with lambda phosphatase (P), or lambda phosphatase + phosphatase inhibitors (P+I) prior to detection by anti-MYC immunoblot. In vitro phosphorylated recombinant Sic1 was used as a control to demonstrate activity of the phosphatase. (D) Absolute Nrs1 concentration in single cells grown and imaged in nitrogen-limited medium (YNB+Pro) as a function of cell size, as determined by sN&B. Blue and orange dots represent individual cells from 2 different experiments. The typical size range of cells at the G1/S transition (800 to 1,000 pixels, corresponding to 27 to 38 fL) is indicated. Cell-averaged total Nrs1 concentration (top) and nuclear concentration where Nrs1 nuclear localization was evident (bottom) are shown. Infrequent small cells with high Nrs1 levels had high autofluorescence and no nuclear localization of the signal. (E) Example of high-content confocal image of Nrs1-GFP cells grown to log phase in nitrogen-limited medium. Arrows indicate example cells with strong (green), dim (blue), or no nuclear Nrs1 (red) or inviable cells (white). The histogram summarizes Nrs1 signals in small unbudded

(708 cells), large unbudded and small-to-medium budded (599 cells) and medium-to-large budded cells (186 cells) from 18 confocal images. Inviable cells with high autofluorescence, out-of-focus cells for which the budding pattern could not be ascertained and regions in which illumination was not homogeneous were not scored. All numerical values underlying panels D and E may be found in S1 Data. NRS1, Nitrogen-Responsive Start regulator 1; sN&B, scanning Number and Brightness; YNB+Pro, YNB + 0.4% proline + 2% glucose.

https://doi.org/10.1371/journal.pbio.3001548.g002

confirmed with an independent fusion of Nrs1 to wild-type GFP (S1D Fig). Hyperosmotic stress, oxidative stress, and DNA damage did not induce Nrs1 expression in SC + 2% glucose medium (S1E and S1F Fig). Immunoblot analysis of a Nrs1^{13MYC} strain in different carbon and nitrogen sources, as well as in rapamycin-treated and saturated cultures, confirmed the specific expression of Nrs1 only under conditions of nitrogen limitation or TORC1 inhibition (Fig 2B). A slow-migrating form of Nrs1 was induced by nitrogen limitation (Fig 2B) and also appeared first upon rapamycin treatment before conversion to the fast-migrating form (S1C Fig). To investigate the nature of this presumptive posttranslational modification (PTM) on Nrs1, we treated Nrs1^{MYC} immunoprecipitates with lambda phosphatase but found that this did not affect the slower-migrating species (Fig 2C). We also did not detect Nrs1-derived phosphopeptides by mass spectrometry (see below; S4 Table). We have not been able to determine the nature of this modification on Nrs1.

Nrs1 abundance peaks at the G1/S transition

We quantified Nrs1-GFP levels in asynchronous populations of live cells grown in nitrogen-limited YNB medium with our custom sN&B analysis software [22]. Nrs1-GFP concentrations, averaged over entire single cells, were between 5 and 20 nM. Higher levels were observed in cells close to the typical critical size at the end of G1 phase, where Nrs1-GFP was predominantly nuclear. In these cases, Nrs1 nuclear concentration was 60 to 80 nM (Fig 2D). These Nrs1 nuclear levels at Start were comparable to Swi4 (50 to 100 nM), Whi5 (100 to 120 nM), and Swi6 (130 to 170 nM) levels determined previously by the same method [22]. We further confirmed Nrs1-GFP expression and nuclear localization principally in large unbudded and small-to-medium budded cells in high-content images acquired by standard confocal microscopy (Fig 2E). The cell cycle–regulated expression pattern of Nrs1 protein suggested that it plays a role at Start, consistent with suppression of the $cln3\Delta$ $bck2\Delta$ arrest by NRS1 overexpression.

NRS1 genetically interacts with SBF and other Start regulators

To investigate the mechanism by which Nrs1 promotes Start, we examined genetic interactions of *NRS1* with the main known Start regulators. Overexpression of *NRS1* from the *GAL1* promoter, either integrated at the *NRS1* locus or from a 2- μ m high copy plasmid [50], caused a pronounced small size phenotype, in agreement with its putative role as a Start activator (Fig 3A and 3B). To interrogate the genetic requirements for this size phenotype, we transformed deletion mutants of known Start regulators with the *GAL1-NRS1* high copy plasmid and examined cell size epistasis. *NRS1* overexpression almost entirely rescued the large size phenotype of a *cln3* Δ mutant and partially rescued the large size of a *bck2* Δ mutant (Fig 3B). A *whi5* Δ mutant was epistatic to *NRS1* overexpression, whereas a *nrs1* Δ deletion did not exacerbate the larger size caused by *WHI5* overexpression and only modestly increased the size of a *whi5* Δ mutant (Fig 3C). Notably, the small size caused by *NRS1* overexpression was abrogated in *swi6* Δ and *swi4* Δ mutant strains (Fig 3D). This requirement for full SBF function was further demonstrated with a temperature-sensitive *swi4-ts* strain in which Swi4 binding to Swi6 is altered [51], grown at the semipermissive temperature of 30°C (Fig 3E).

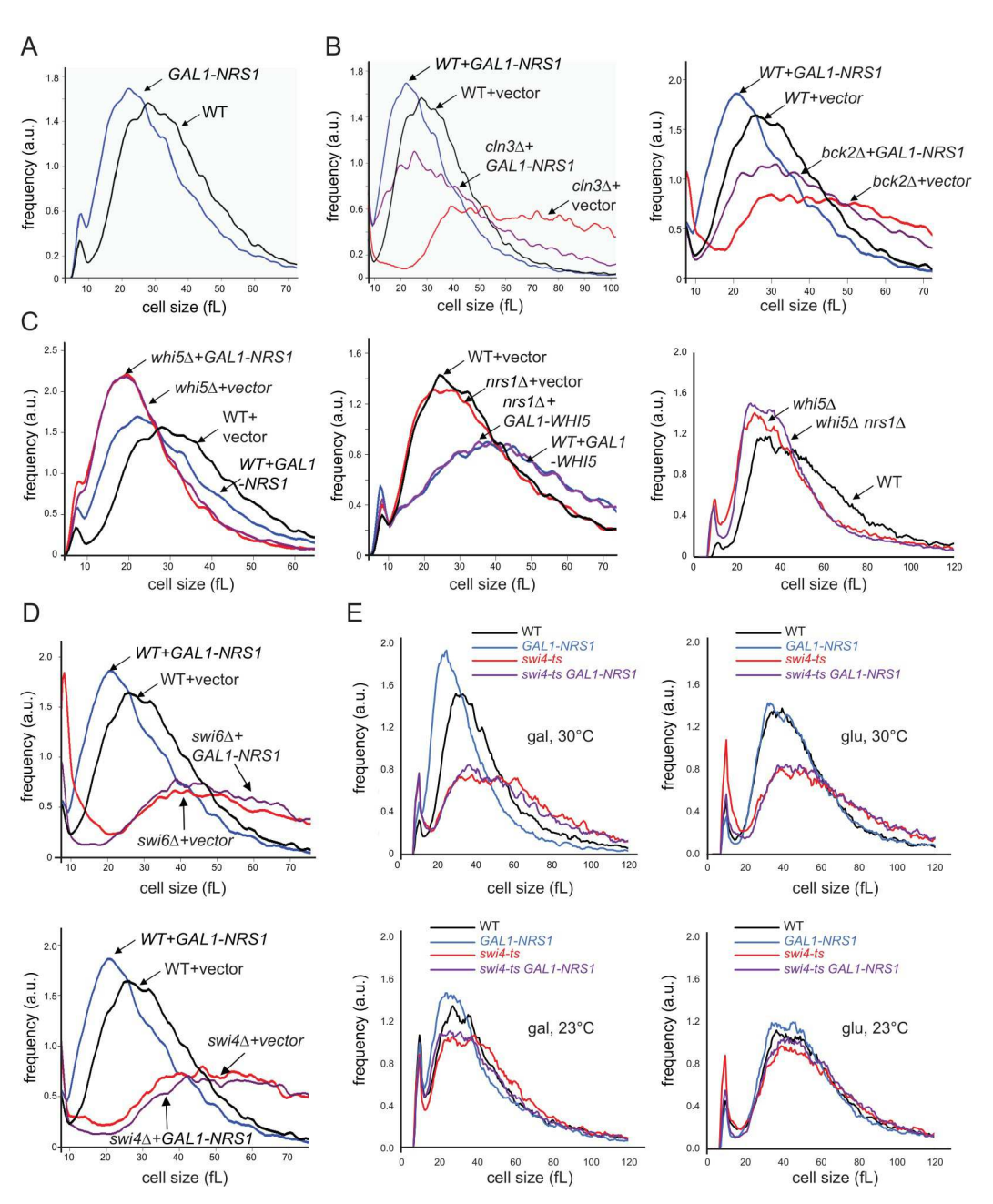


Fig 3. NRS1 is genetically upstream of SBF. Cell size distributions were determined for the indicated genetic combinations. (A) NRS1 overexpression alone. (B) NRS1 overexpression with either $cln3\Delta$ or $bck2\Delta$ mutations. (C) NRS1 overexpression and $nrs1\Delta$ mutation with either WHI5 overexpression or $whi5\Delta$ mutation. (D) NRS1 overexpression with either $swi4\Delta$ or $swi6\Delta$ mutations. (E) NRS1 overexpression with a swi4-ts mutation. Strains were transformed with either GAL1-NRS1, GAL1-WHI5, or empty vector control high copy plasmids as indicated. Strains bearing galactose-regulated constructs and associated controls were induced for 6 hours in SC + 2% galactose before size determination. WT plots shown in panels B, C, and D (left, middle) represent the same measurement. All numerical values underlying this figure may be found in S2 Data. NRS1, Nitrogen-Responsive Start regulator 1; SBF, SCB-binding factor; WT, wild-type.

https://doi.org/10.1371/journal.pbio.3001548.g003

In contrast to its overexpression, deletion of *NRS1* did not detectably affect overall growth rate or cell size in a wild-type S288C (BY4741) laboratory strain, regardless of whether cells were grown in either nitrogen-replete or nitrogen-limited medium (S2A–S2D Fig). Moreover, in competitive growth experiments, $nrs1\Delta$ and wild-type cells had indistinguishable fitness

(S1 Text and S2E Fig). Because the small size phenotype caused by NRS1 overexpression depended on SWI4 and SWI6, we hypothesized that MBF might partially compensate for loss of *NRS1* function. We therefore generated an $mbp1\Delta nrs1\Delta$ double mutant strain and evaluated growth in nitrogen-rich SC and nitrogen-poor YNB+Pro media. While the single mutant strains had no growth defect in either condition, the $mbp1\Delta nrs1\Delta$ double mutant had a pronounced growth defect that was specific to nitrogen-poor conditions (Fig 4A). We furthermore considered the possibility that laboratory strains may have lost some requirements for NRS1 through the course of decades-long propagation in artificially rich nutrient conditions. To test this idea, we deleted NRS1 in the prototrophic wild yeast Saccharomyces boulardii, which shares >99% of its genome with S. cerevisiae including NRS1 [52]. An S. boulardii strain lacking NRS1 grew slower than wild-type cells in nitrogen-poor medium specifically (i.e., YNB+Pro+0.1% glucose medium not supplemented with amino acids, Fig 4B). Hence, under conditions of nitrogen limitation, NRS1 promotes growth in genetically crippled contexts in laboratory strains and is required for optimal growth of a wild variant of S. cerevisiae. Taken together, these genetic interactions suggested that Nrs1 promotes the G1/S transition by acting upstream of the Whi5-inhibited form of SBF in a manner that is independent of Cln3 and Bck2.

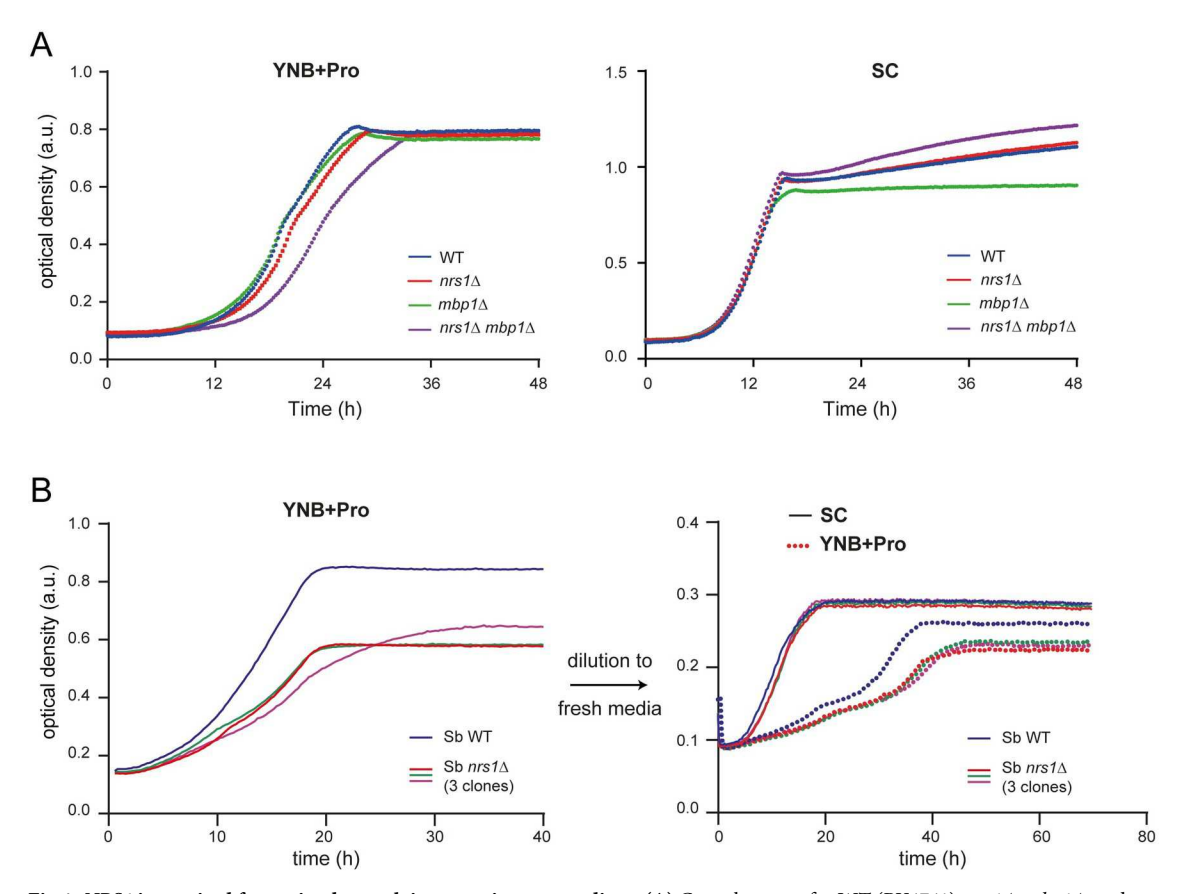


Fig 4. NRS1 is required for optimal growth in poor nitrogen medium. (A) Growth curves for WT (BY4741), $nrs1\Delta$, $mbp1\Delta$, and $mbp1\Delta$ $nrs1\Delta$ laboratory strains grown in nitrogen-limited YNB+Pro+0.1% glucose medium and nitrogen-rich SC+0.1% glucose medium. Curves represent the average of 3 different clones for each mutant strain. (B) Growth curves for WT and $nrs1\Delta$ S. boulardii strains were grown in either nitrogen-poor YNB+Pro+0.1% glucose minimal medium (i.e., not supplemented with any other amino acids) or nitrogen-rich SC+0.1% glucose medium. Three different isolates for the $nrs1\Delta$ S. boulardii strain were analyzed. Growth curves are the average of at least 12 independent colonies for each strain. To eliminate potential nutrient lag effects, cultures were rediluted into fresh medium, and their growth was monitored again. All numerical values are provided in S3 Data. NRS1, Nitrogen-Responsive Start regulator 1; WT, wild-type; YNB+Pro, YNB + 0.4% proline + 2% glucose.

https://doi.org/10.1371/journal.pbio.3001548.g004

Nrs1 interacts with SBF in vivo and in vitro

We next sought to identify Nrs1 protein interactors under conditions in which Nrs1 was endogenously expressed at physiological levels. We performed immunoaffinity purification on lysates from an endogenously tagged NRS1^{13MYC} strain and a control untagged strain grown in nitrogen-limited YNB+Pro medium. Analysis of the samples by mass spectrometry (see Methods and S1 Text) identified multiple peptides (S4 Table) from which the corresponding proteins were identified (>2 unique peptides, false discovery rate [FDR] <1%, <u>S5 Table</u>). Proteins specific to the Nrs1^{13MYC} sample were identified by subtracting proteins present in the untagged control and filtering hits against the CRAPome database of nonspecific interactions [53]. This workflow yielded 7 proteins that were specific to the Nrs1^{13MYC} sample (S3 Table and S3A Fig). Of these, Nrs1 was represented by 7 peptides (48% coverage), Swi4 by 5 peptides, and Swi6 by 5 peptides; the remaining 4 candidates were represented by only 2 or 3 peptides and thus of lower confidence. This unbiased analysis demonstrated that endogenous Nsr1 expressed under physiological conditions interacted with SBF. To confirm this result, we performed co-immunoprecipitation experiments on extracts of rapamycin-treated cells expressing either SWI4^{3FLAG} or SWI6^{3FLAG} alleles in combination with either NRS1^{13MYC} or WHI5^{13MYC} alleles, each expressed from their respective endogenous promoter. Swi4^{3FLAG} and Swi6^{3FLAG} were each immunoprecipitated with anti-FLAG resin and then blotted with antibodies against either FLAG or MYC epitope tags. Nrs1^{13MYC} and Whi5^{13MYC} were detected in immunoprecipitates of endogenous Swi4^{3FLAG} and Swi6^{3FLAG} from cells grown the presence of rapamycin but not in control immunoprecipitates from strains that lacked the FLAG-tagged alleles (Figs 5A and S3B). A similar experiment carried out with polyclonal anti-Swi4 and anti-Swi6 antibodies specifically detected endogenous SBF in Nrs1 13MYC immunoprecipitates from cells grown in the presence but not the absence of rapamycin (S3C Fig). Collectively, these results suggested that Nrs1 directly interacted with SBF under physiological conditions.

To determine if the interaction between Nrs1 and SBF was direct, we carried out *in vitro* binding assays with purified recombinant proteins. We titrated recombinant FLAG Swi4-Swi6 and FLAG Mbp1-Swi6 complexes produced in baculovirus-infected insect cells [12] against recombinant GST Nrs1 produced in *E. coli* and immobilized on GSH-Sepharose resin. Swi4 and Swi6 were both captured with GST Nrs1 across the titration series, whereas control GSH-Sepharose resin did not bind SBF (Fig 5B). In contrast, GST Nrs1 did not detectably interact with the FLAG Mbp1-Swi6 complex under the conditions tested, suggesting that specificity for Nrs1 is determined by the DNA-binding subunit and not the common Swi6 subunit of SBF/MBF. To test whether Nrs1 was able to interact with Whi5-bound SBF, we titrated purified recombinant GST Nrs1 into a preformed recombinant GST Whi5-FLAG Swi4-Swi6 complex. We observed that Nrs1 bound effectively even in the presence of Whi5 (Fig 5C). These results demonstrated that endogenous Nrs1 interacts directly and specifically with the Swi4-Swi6 complex, that no additional factors are needed for this interaction to occur, and that Nrs1 can bind SBF even in the presence of Whi5.

Nrs1 binds to SBF-regulated promoters in vivo

We next assessed the presence of Nrs1^{13MYC} at the SBF-regulated promoters of CLN2 and PCL1 by chromatin immunoprecipitation (ChIP). For both genes, we specifically detected SCB-containing promoter sequences by PCR in cross-linked anti-MYC immune complexes purified from cells that expressed Nrs1^{13MYC} from the endogenous NRS1 locus (Fig 6A). The enrichment of PCL1 and CLN2 sequences in Nrs1^{13MYC} immunoprecipitates only in rapamy-cin-treated cells further demonstrated that Nrs1 specifically binds SBF-regulated G1/S promoter DNA (Fig 6A).

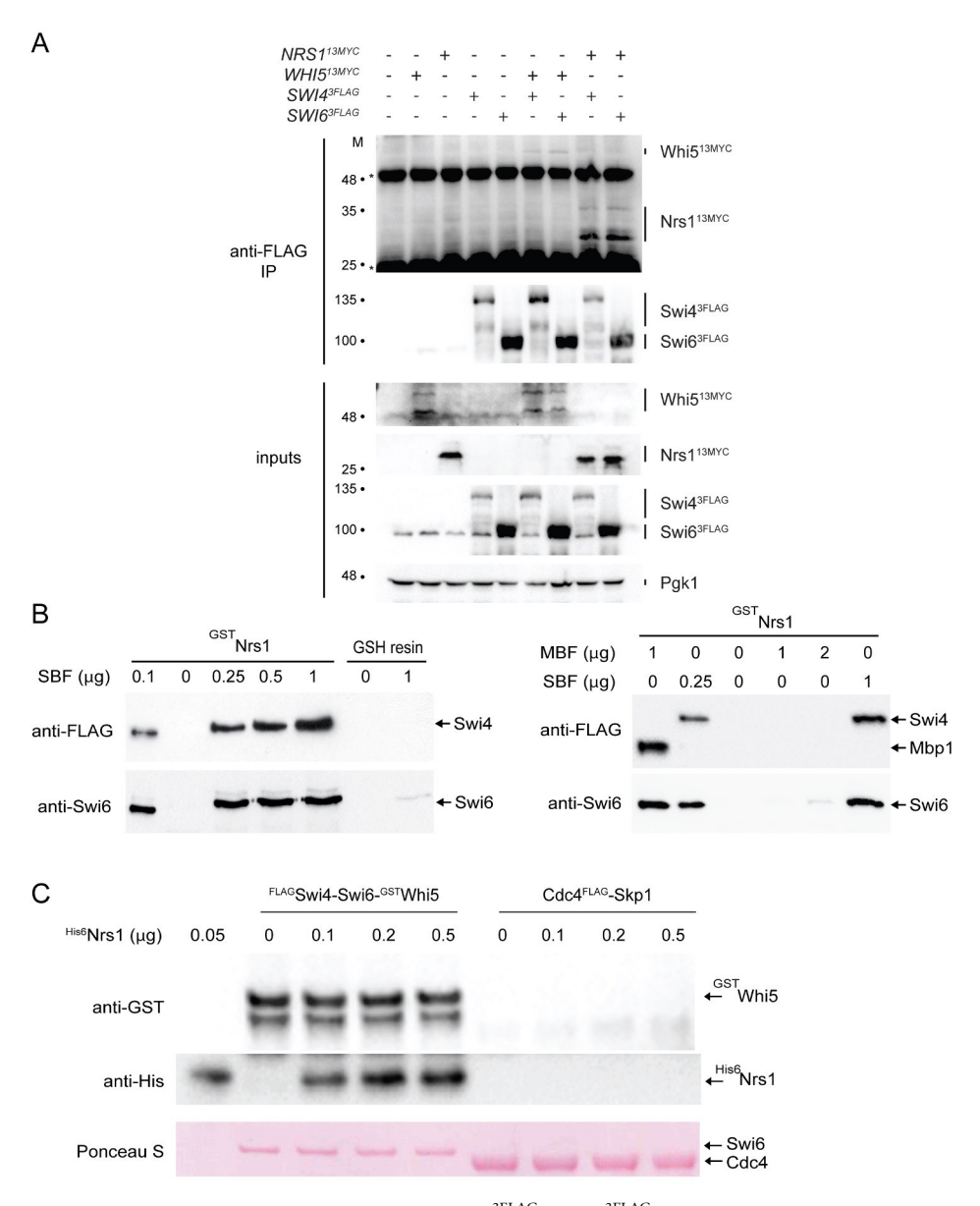


Fig 5. Nrs1 binds to SBF in vivo and in vitro. (A) Swi4^{3FLAG} or Swi6^{3FLAG} complexes were immunoprecipitated from the indicated strains grown in the presence of 200 nM rapamycin for 2 hours and interacting proteins assessed by immunoblot with the antibodies against the indicated tags or proteins. Co-immunoprecipitation of Whi513MYC with Swi4^{3FLAG} and Swi6^{3FLAG} served as a positive control. Mr markers (M) are indicated for each blot. Pgk1 served as a loading control. Note the lower Mr form of Whi5 visible in the input blot is obscured by the IgG heavy chain signal in the immunoprecipitations. Data is representative of at least 5 independent experiments (see $\underline{S3B \ Fig}$ for a replicate experiment and $\underline{S3C \ Fig}$ for a reciprocal Nrs1 13MYC and Whi5 13MYC co-immunoprecipitation experiment performed with polyclonal anti-Swi4 and anti-Swi6 antibodies). (B) Recombinant GSTNrs1 immobilized on GSH-Sepharose resin was incubated with increasing concentrations of soluble purified SBF (FLAGSwi4-Swi6) or MBF (FLAGMbp1-Swi6). Bound proteins were analyzed by immunoblot with anti-Swi6 and anti-FLAG antibodies as indicated. GSH-Sepharose resin alone served as a negative control. (C) Recombinant FLAGSwi4-Swi6-GSTWhi5 complexes containing 0.1 ug of $^{
m GST}$ Whi5 were incubated with increasing amounts of recombinant ${
m His}_6$ -tagged Nrs1 (0.1 ug, 0.2 ug, and 0.5 ug, equivalent to 4, 8, and 20 Nrs1:Whi5 molar ratio), immunoprecipitated using anti-FLAG beads to capture SBF-Whi5 complexes and probed with anti-GST antibody to detect Whi5 and anti-HIS6 antibody to detect Nrs1. Coimmunoprecipitation with an irrelevant recombinant protein complex (Cdc4-FLAGSkp1) on anti-FLAG beads served as a negative control for interaction specificity. Ponceau S stain was used to demonstrate equivalent input protein complexes in each lane. Raw images of all original immunoblots are provided in the S1 Raw Images. MBF, MCB-binding factor; NRS1, Nitrogen-Responsive Start regulator 1; SBF, SCB-binding factor.

https://doi.org/10.1371/journal.pbio.3001548.g005

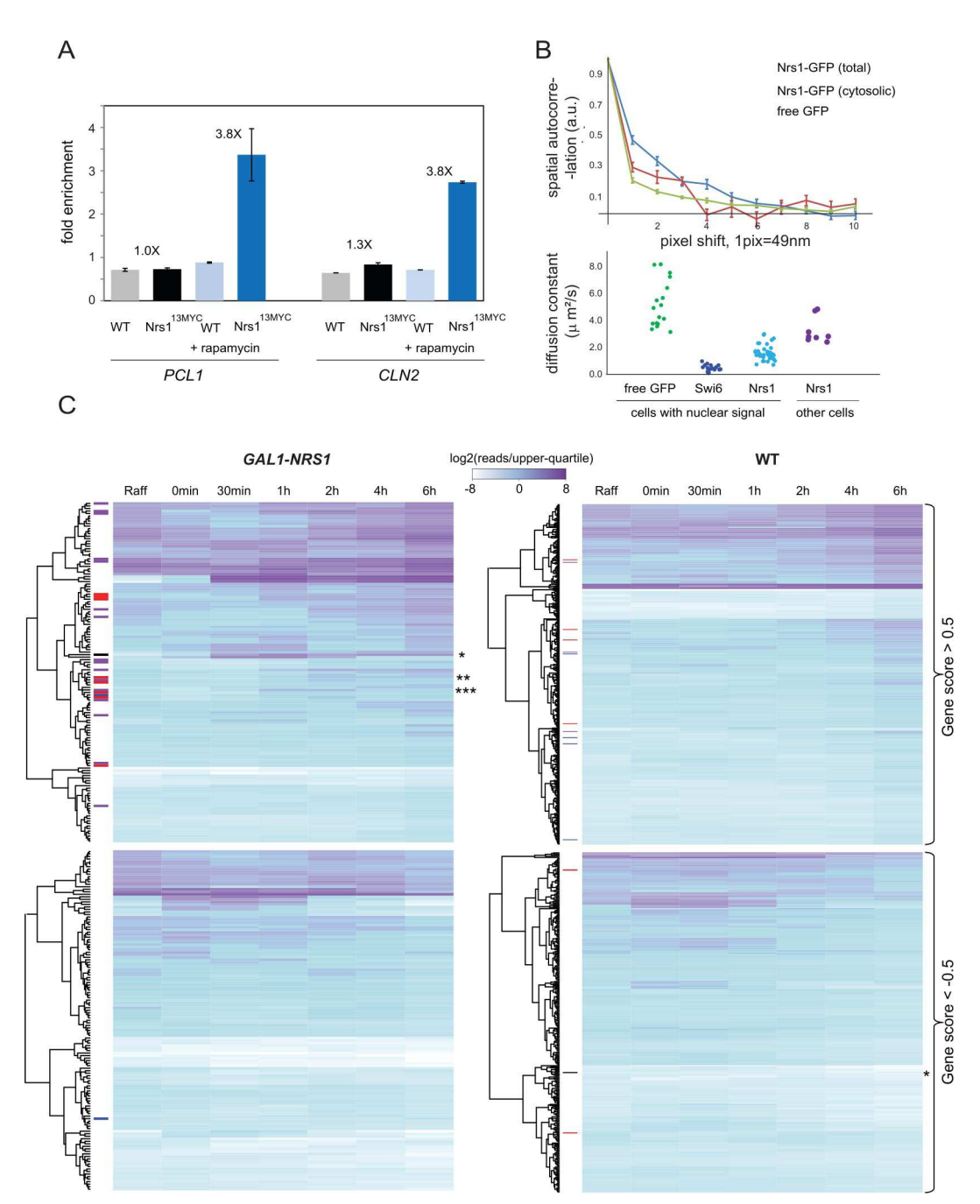


Fig 6. Nrs1 binds to SBF-regulated promoter DNA and activates SBF-driven transcription. (A) Anti-MYC chromatin immunoprecipitates from WT untagged control and $NRS1^{I3MYC}$ strains either untreated or treated with 200 ng/mL rapamycin for 2 hours were probed for the presence of CLN2 and PCL1 promoter DNA sequences by real-time quantitative PCR. Bars indicate the mean fold-enrichment across 2 replicates, and error bars show the standard error on the mean. (B) Top panel: RICS vertical correlations from a NRS1-GFP strain grown in nitrogen-limited medium (YNB+Pro) as a function of the pixel shift for total and cytosolic Nrs1-GFP pools. RICS correlation for free GFP was used as a control for unconstrained diffusion. Data points show correlation averages over N FOV (N = 25 for nuclear Nrs1, N = 7 for cytosolic Nrs1, N = 12 for free GFP). Each FOV contained 1 to 5 cells. Error bars represent the standard error on the mean. Bottom panel: Scatter plots of fitted diffusion coefficients from individual FOVs of the same strains. Data from Swi6-GFP FOVs served as a control for constrained diffusion. All numerical values underlying panels A and B may be found in <u>S5 Data</u>. (C) Heatmaps of gene expression profiles upon galactose induction of GAL1-NRS1 and WT control strains. Genes were selected based on a gene rank score across biological triplicates and values shown are upper quartile-normalized log2-read counts averaged across triplicates for each time point. Genes that were strongly up-regulated (gene score < 0.5) and down-regulated (gene score < 0.5) are shown. Genes were clustered for GAL1-NRS1 and WT heatmaps separately according to the default

settings of the R Heatmap function. Positions of NRS1 (*), CLN2 (**), and PCL1 (***) are indicated. SBF (red), MBF (blue), and SBF/MBF (purple) target genes are indicated on the left side. Raw data underlying this panel may be found on the Gene Expression Omnibus database under the accession number GSE179366. FOV, field of view; MBF, MCB-binding factor; NRS1, Nitrogen-Responsive Start regulator 1; RICS, raster image correlation spectroscopy; SBF, SCB-binding factor; WT, wild-type; YNB+Pro, YNB + 0.4% proline + 2% glucose.

https://doi.org/10.1371/journal.pbio.3001548.g006

We predicted that Nrs1 binding to chromatin should reduce Nrs1 mobility in the nucleus. To test this hypothesis, we assessed the molecular dynamics of Nrs1-GFP in cells grown in nitrogen-limited medium using raster image correlation spectroscopy (RICS). The RICS method exploits the hidden time structure of imaging scans, in which adjacent pixels are imaged a few microseconds apart, to quantify the diffusional properties of fluorescent molecules [54–56]. Intensity correlations between pixels shifted along the direction of scanning (horizontal correlations), and along the orthogonal direction (vertical correlations), are averaged over multiple scans. Horizontal and vertical correlations that decay with increasing pixel shift are characteristic of the dynamical properties on 10 to 100 µs and 5 to 50 ms timescales, respectively. We found that the vertical RICS correlations of nuclear Nrs1-GFP signal decreased on a slower timescale than either free nuclear GFP or cytosolic Nrs1-GFP signal (Fig 6B). Fitted Nrs1-GFP diffusion coefficients in cells in which Nrs1 was predominantly nuclear were lower compared to cells in which it was mostly cytosolic and also lower than the diffusion coefficient of free nuclear GFP, a proxy for free diffusion in the nucleus. The Nrs1 diffusion coefficient was similar to that of Swi6-GFP which is largely DNA bound (Fig 6B). This result indicated that Nrs1 associates with a slow-moving nuclear component, most likely chromatin.

The apparent size epistasis between *whi5∆* and *GAL1-NRS1* prompted us to ask whether Nrs1 might reduce the association Whi5 with SBF and/or chromatin. However, ChIP analysis of Whi5^{HA} at the *CLN2* and *PCL1* promoters revealed that Whi5^{HA}−promoter interactions were not reduced in the presence of overexpressed *NRS1* (S4A Fig). In addition, *GAL1-NRS1* cells had wild-type levels of Whi5 as determined by sN&B quantification (S4B Fig), and *GAL1-NRS1* did not alter Whi5^{HA} association with Swi4 or Swi6 in co-immunoprecipitation experiments (S4C Fig). Nrs1 and Whi5 also did not compete for SBF binding in *in vitro* binding assays with recombinant proteins (S4D Fig). Together, these results obtained using different *in vivo*, *in vitro*, biochemical, and imaging-based approaches suggested that Nrs1 binds SBF at G1/S promoters *in vivo*, but that the binding of Nrs1 does not alter Whi5 interactions with SBF or promoter DNA. These results led us to consider the possibility that Nrs1 might directly activate transcription.

Ectopic expression of NRS1 activates the G1/S regulon

To assess the potential role of Nrs1 in transcription, we used RNA sequencing (RNA-seq) to determine the genome-wide transcriptional response to ectopic *NRS1* overexpression. Three biological replicates of *nrs1*::*GAL1-NRS1* and wild-type cells were grown to log-phase in SC +2% raffinose medium, induced with galactose for 6 hours, and transcriptional profiles analyzed by RNA-seq. Gene scores were defined based on their expression fold-change before and after 6-hour induction, comparing for each gene the fold-change across multiple replicates to control for intersample expression variability and the effects of galactose (see Methods; all scores provided in S6 Table). Up-regulated genes in the *GAL1-NRS1* samples included *NRS1* itself as expected (rank 1) and many of the 139 SBF/MBF target genes that comprise the G1/S regulated genes [10]. These G1/S genes included *CLN2* (rank 12) and *PCL1* (rank 82), the promoters of which were bound by Nrs1 as shown above. Nrs1 also strongly induced the expression of *HO*

(rank 10), *RNR1* (rank 15), and *HCM1* (rank 20), which are markers of the G1/S transition. Visualization of the data in a heatmap format illustrated the overall enrichment of SBF/MBF target genes (Fig 6C). Among the most strongly up-regulated genes (score >0.5), SBF targets were enriched 12-fold compared to random expectation (24 of 86 genes, $p = 3*10^{-20}$), MBF targets were enriched 7-fold (17 of 101 genes, $p = 9*10^{-11}$), but out of the 17 strongly up-regulated MBF targets, 16 were also SBF targets so that MBF-only targets were not enriched (1/53 genes, p = 0.65). In the wild-type control samples, no significant enrichment/depletion compared to random expectations was observed. We note that in addition to recognition of its cognate SCB elements, SBF can also activate genes that only contain MCB elements [57] such that the apparent specificity of Nrs1 for SBF is not undermined by the up-regulation of MBF genes in these experiments.

Nrs1 confers transcriptional activity that can rescue G1/S-transcription deficient mutants

We next asked whether Nrs1 might itself function directly as a transcriptional activator. To test this hypothesis, we constitutively expressed a Nrs1-Gal4 DNA-binding domain fusion protein ($GAL4^{DBD}$ -NRS1) in a reporter strain bearing the HIS3 gene under control of the GAL1 promoter. We used $GAL4^{DBD}$ alone and $GAL4^{DBD}$ fused to an irrelevant human gene (UBE2G2) that potently transactivates as negative and positive controls, respectively. Full-length NRS1, but not a truncated version that encoded only the conserved carboxyl terminus, was able to activate transcription of the HIS3 reporter and thereby allow cell growth in medium lacking histidine (Figs 7A and 85A).

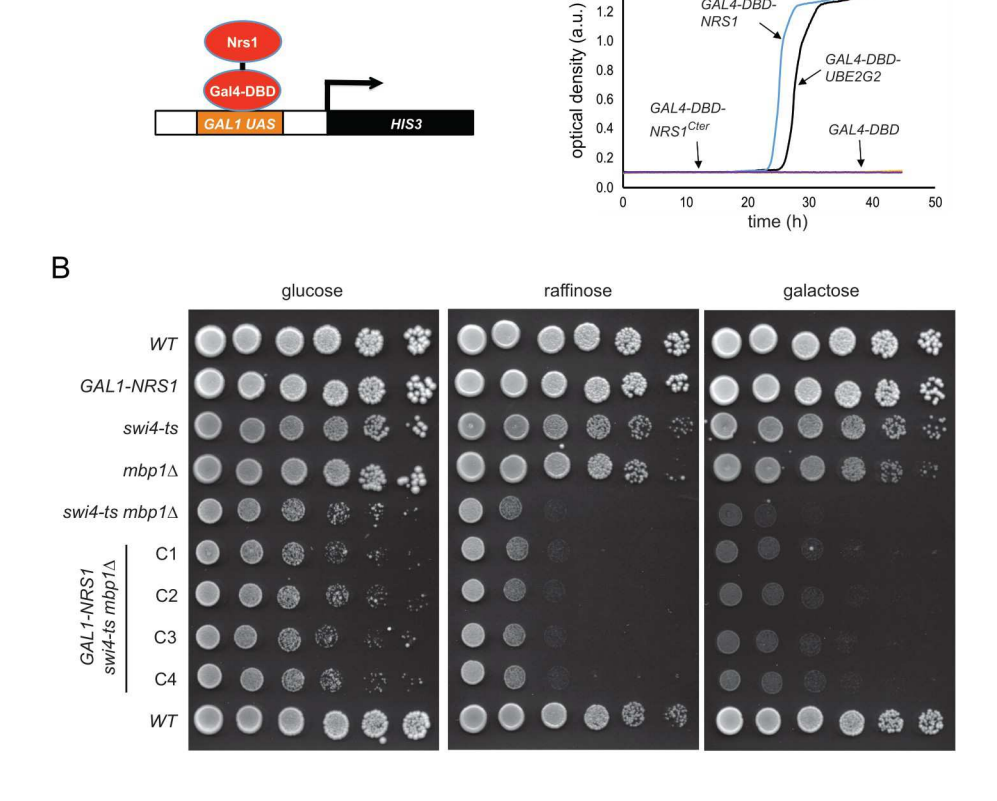
Given the inherent transactivation capacity of Nrs1, we next investigated whether NRS1 overexpression could suppress the growth defects caused by loss of other G1/S activators. We first tested a cln1Δ cln2Δ cln3Δ MET-CLN2 strain, in which G1 cyclin activity is restricted to methionine-free media, with or without a pGAL1-NRS1> plasmid. Repression of CLN2 by methionine caused a growth arrest, whether or not NRS1 was expressed, although ectopic expression of NRS1 did modestly reduce cell size and slightly increased cell proliferation (S5B) Fig). Hence, NRS1 cannot compensate for the total lack of G1-cyclin activity. We then tested whether NRS1 overexpression could suppress the growth defects of mutants in which G1/S transcription was impaired, but in which Cln-Cdc28 activity was preserved. We first tested a $mbp1\Delta$ swi4-ts double mutant [58]. The growth of a GAL1-NRS1 $mbp1\Delta$ swi4-ts strain was improved with respect to the $mbp1\Delta$ swi4-ts control at a semipermissive temperature of 30° in galactose medium (Fig 7B; see S5C Fig for plate images with a 2-day extension of the incubation period), but not in other media or at the fully permissive temperature (S5B Fig). As a further test, we examined NRS1-mediated suppression in strains that expressed WHI5^{12A} and SWI6^{SA4} alleles in which all Cdc28 consensus sites are mutated, a combination that abrogates the Cln-Cdc28 mediated relief of SBF inhibition by Whi5 [12,14]. Overexpression of NRS1 also partially rescued the growth defect of this strain (Fig 7C). These results suggested that Nrs1 provides an alternative mechanism of Start activation by augmenting G1/S transcription in the presence of Whi5-mediated inhibition.

Nrs1 can bypass Whi5 inhibition of SBF

To test whether physiological levels of Nrs1 targeted to SBF are sufficient to promote Start activation, we constructed a strain expressing a Whi5-Nrs1-GFP fusion protein from the endogenous *WHI5* promoter. Experiments with this strain were carried out in SC complete medium to avoid other possible nitrogen-dependent parallel inputs to Start and to focus on Nrs1 function. The chimeric protein was expressed and had the expected molecular mass (S6A Fig) and

Α

GAL4-DBD-



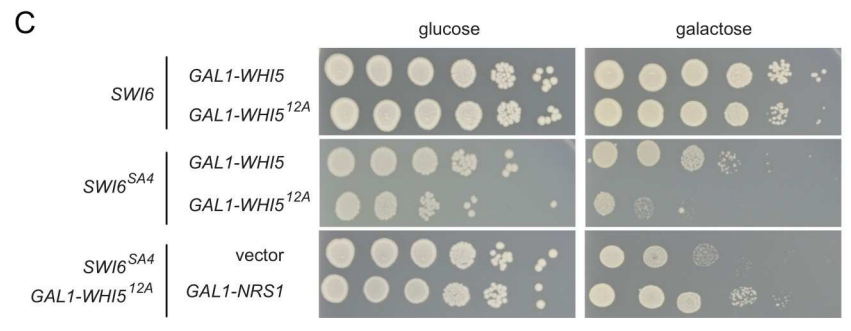


Fig 7. Nrs1 has an inherent transcription activation function that can partially rescue G1/S-transcription deficient mutants. (A) Transactivation of a HIS3 reporter by fusion of Nrs1 to the Gal4 DNA-binding domain (GAL4^{DBD}-NRS1) but not by fusion of the Nrs1 carboxyl terminus (GAL4^{DBD}-NRS1^{Cter}). GAL4^{DBD}-UBE2G2 and GAL4^{DBD} constructs served as positive and negative controls, respectively. Growth curves were determined in -His -Trp medium. All numerical values underlying this panel may be found in S6 Data. (B) Serial 5-fold dilutions of NRS1 and GAL1-NRS1 strains in WT, swi4-ts, $mbp1\Delta$, and $mbp1\Delta swi4$ -ts backgrounds were spotted onto SC + 2% glucose, SC + 2% raffinose and SC + 2% galactose, and grown for 5 days at 30°C. C1 to C4 indicate 4 independent clones of the mbp1Δ swi4-ts GAL1-NRS1 strain. (C) Serial 5-fold dilutions of WT or swi6Δ strains transformed with GAL1-WHI5, GÂL1-WHI5^{12A}, GAL1-SWI6^{SA4}, GAL1-NRS1, or empty control plasmids or combinations thereof were spotted on rich medium containing 2% glucose or 2% galactose and grown for 2 days at 30°C. NRS1, Nitrogen-Responsive Start regulator 1; WT, wild-type.

https://doi.org/10.1371/journal.pbio.3001548.g007

retained the localization pattern of endogenous Whi5, with about 30% to 35% of pre-Start cells showing a prominent nuclear signal (Figs 8A and S6B). Cells expressing Whi5-Nrs1-GFP were almost as small as whi5∆ cells (Fig 8B). This phenotype was not due to the presence of the GFP tag since size distributions of strains expressing untagged versus GFP-tagged Whi5 were

indistinguishable (S6C Fig). Moreover, cells expressing the chimeric protein grew at the same rate as wild-type and $whi5\Delta$ strains (S6D Fig). Strikingly, cells expressing Whi5-Nrs1-GFP were as small as cells that expressed GAL1-NRS1 in galactose medium (Fig 8C).

As a reduction of Whi5 dosage in the Whi5-Nrs1-GFP fusion context could in principle explain the small size of this strain, we used sN&B to compare the nuclear concentrations of Whi5 in the wild-type and the Nrs1-fusion contexts. Whi5 levels in wild-type cells were 110 to 130 nM, consistent with those determined previously [22]. The Whi5-Nrs1-GFP chimera was present at a slightly lower concentration, 80 to 100nM (Fig 8A), close to endogenous Nrs1 nuclear levels in nitrogen-limited media (60 to 80 nM, see Fig 2D). This slight decrease in Whi5 abundance was unlikely to explain the small size of cells expressing Whi5-Nrs1-GFP since cell size is not strongly sensitive to *WHI5* gene dosage [25,59]. We confirmed that hemizygous *WHI5/whi5*\D diploid cells were only marginally smaller than wild-type diploid cells (S6E Fig) and, moreover, *WHI5* overexpression only causes a 20% to 30% increase in mode size (Fig 3C), in agreement with previous results [25,59]. Consistently, our previously published Start model [22] also predicted that down-regulating Whi5 levels from 120nM to 85nM should not affect the critical size at Start (S6F Fig).

Finally, we predicted that the Whi5-Nrs1 fusion should be sufficient to rescue the lethal Start arrest of a $cln3\Delta$ $bck2\Delta$ strain. We crossed a $cln3\Delta$ strain bearing the integrated WHI5-NRS1-GFP allele to a $bck2\Delta$ strain and analyzed growth of dissected tetrads on selective media to identify spore genotypes (Fig 8D). We recovered many viable $cln3\Delta$ $bck2\Delta$ WHI5-NRS1-GFP triple mutant spore clones but did not recover any viable $cln3\Delta$ $bck2\Delta$ WHI5 double mutant clones (Fig 8D). As expected, no viable $cln3\Delta$ $bck2\Delta$ spore clones were obtained from a control cross of a $cln3\Delta$ whi5::WHI5-GFP and a $bck2\Delta$ strain (Fig 8D). As a further control to ensure that the Nrs1 fusion did not merely inactivate Whi5 in a nonspecific manner, we fused the above transcriptionally inactive carboxyl-terminal fragment of Nrs1 to Whi5 and showed that it did not reduce cell size (S7A Fig) nor rescue the $cln3\Delta$ $bck2\Delta$ lethality (S7B Fig). These results supported a model in which Nrs1 bypasses Whi5 inhibition by directly conferring transactivation activity on the Whi5-inhibited SBF complex.

Discussion

On the premise that additional genes may activate Start under suboptimal nutrient conditions, we screened for genes that can circumvent the Start arrest caused by loss of both CLN3 and BCK2 function. We discovered that NRS1 overexpression efficiently bypasses the lethality of a $cln3\Delta$ $bck2\Delta$ strain and activates Start in wild-type cells; that Nrs1 associates with SBF at G1/S promoter DNA and promotes SBF-dependent transcription; that NRS1 overexpression can genetically suppress defects in SBF function; and that Nrs1 is itself a transcriptional activator. Our data suggest a model whereby nitrogen limitation or TORC1 inhibition promote NRS1 expression and that Nrs1 binding to SBF directly recruits the transcriptional machinery to overcome Whi5-mediated inhibition of SBF (Fig 8E). In effect, endogenous Nrs1 acts as a nutrient-dependent parallel input into SBF. Although this input appears dispensable under most growth conditions, it is revealed in a genetically sensitized context in laboratory strains and in wild yeast strains. We stress that the $cln3\Delta$ $bck\Delta$ GAL1-WHI5 parental background used for the original high copy suppression screen might have biased towards the discovery of Start activators able to operate in presence of high Whi5 dosage.

This model of Nrs1 function (Fig 8E) allows reinterpretation of some previous *YLR053c/NRS1* genetic interactions uncovered in high-throughput studies [60]. Deletion of *NRS1* slightly aggravates the growth defect of a *ESS1* prolyl isomerase mutation which, in turn, exhibits negative genetic interactions with deletions of *SWI6* or *SWI4* [61]. Although the latter

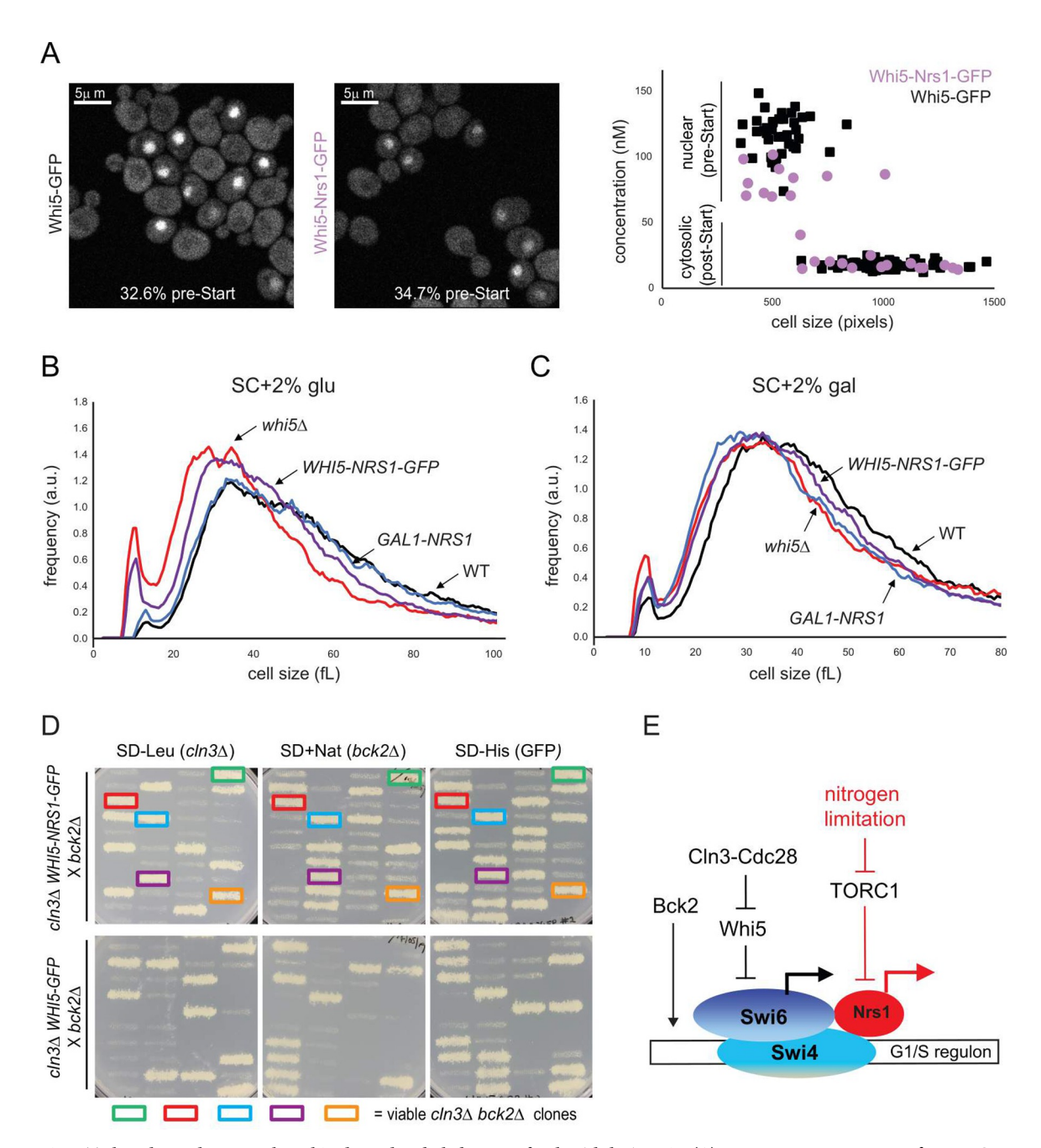


Fig 8. Tethered Nrs1 bypasses the Whi5-dependent lethal arrest of a *cln3Δ bck2Δ* strain. (A) sN&B microscopy images of *WHI5-GFP* and *WHI5-NRS1-GFP* cells grown in SC + 2% glucose. Scale bars are 5 μm. The same intensity scale was used on both images. Fractions of pre-Start G1 cells were computed based on the assessment of nuclear GFP signal in *WHI5-GFP* cells (*N* = 245) and *WHI5-NRS1-GFP* (*N* = 95) cells. Absolute concentrations of Whi5-GFP and Whi5-Nrs1-GFP are shown in the plot. (B) Cell size distributions of WT, *GAL1-NRS1*, *whi5Δ*, and *WHI5-NRS1-GFP* strains in SC + 2% glucose. (C) Cell size distributions of WT, *GAL1-NRS1*, *whi5Δ*, and *WHI5-NRS1-GFP* strains in SC + 2% glucose. (C) Cell size distributions of WT, *GAL1-NRS1*, *whi5Δ*, and *WHI5-NRS1-GFP* X *bck2Δ* cross (top) and a *cln3Δ WHI5-GFP* X *bck2Δ* cross (bottom). For each tetrad, spore clone growth was assessed on SD-LEU (indicates *cln3::LEU2*), SC+NAT (indicates *bck2::NAT*^R), and SD-HIS (indicates *whi5::WHI5-NRS1-GFP-HIS3* or *whi5::WHI5-GFP-HIS3*). Colored boxes indicate viable *cln3Δ bck2Δ* spore clones, all of which also contained the *WHI5-NRS1-GFP* construct. (F) Simplified schematic for Nrs1-dependent activation of Start. Red lines indicate nitrogen-limited conditions. Not all components of the Start machinery are shown. See text for details. *NRS1*, Nitrogen-Responsive Start regulator 1; sN&B, scanning Number and Brightness; WT, wild-type.

https://doi.org/10.1371/journal.pbio.3001548.g008

interactions suggested a possible role of Ess1 in Swi6/Whi5 nuclear import, we did not observe mis-localization of Swi4, Swi6 or Whi5 in either *GAL1-NRS1* or *nrs1*\(\Delta\) strains. With respect to interactions with the transcriptional machinery, *NRS1* overexpression exacerbates the defect caused by deletion of *CTK1*, the catalytic subunit of RNA Pol II carboxyl-terminal domain (CTD) kinase I [62]. In contrast, *NRS1* deletion shows a positive genetic interaction with the RNA Pol II CTD-associated phosphatase, FCP1, which negatively regulates transcription [63]. *NRS1* overexpression also subtly increases chromosomal instability [64], which might result from premature Start activation [65]. These interactions with transcriptional regulators are consistent with our proposed model for Nrs1 function in G1/S transcription activation.

NRS1 is a member of a newly described class of genetic elements variously called protogenes, neo-ORFs, smORFS, small ORF encoded peptides (SEPs), or microproteins [43,66-74]. Computational predictions and ribosomal footprinting first identified hundreds of short species-specific translated peptides from extragenic regions in yeast [43]. Subsequent approaches have yielded a plethora of microproteins encoded by smORFs in various species [66–69,75]. Ribosome profiling and high-throughput genetic analyses has revealed hundreds of functional microproteins in human cells [76,77]. Documented functions for microproteins include phagocytosis [70], autophagy [71], actin-based motility [72], mRNA decapping [78], proteolytic processing [79], mitotic chromosome segregation [73], mitochondrial morphology control [76], plant hormone signaling [80], transcriptional control [81], and cancer cell survival [77], among many others [82,83]. Microproteins derived from noncanonical coding regions represent a substantial fraction of major histocompatibility complex (MHC) class I-associated tumor-specific antigens [84,85]. De novo appearance of short proto-genes coupled with rapid evolution may form a dynamic reservoir for genetic innovation and diversification [43]. Interestingly, lncRNAs appear to evolve rapidly from junk transcripts and, in turn, many lncRNAs appear to encode microproteins [86–88], consistent with the idea that such regulatory functions can readily emerge de novo. Fast evolving genes often have complex expression patterns compared to highly conserved genes and tend to be enriched for transcription-associated functions [89]. The rewiring of transcription factor function by microprotein partners may augment the inherent evolvability of transcriptional control by promoter binding site mutations [90]. As illustrated by the example of NRS1, transcription activation may be a particularly facile route for proto-genes to quickly acquire important regulatory functions that optimize fitness under specific conditions.

Methods

Yeast strains construction and culture

All *S. cerevisiae* strains were isogenic with the S288C (BY4741) auxotrophic background (\$2 Table). Standard molecular genetics methods were employed for genomic integration of carboxyl-terminal tagging cassettes [91] and verified by PCR or sequencing. Standard media were used for yeast growth: rich (XY: 2% peptone, 1% yeast extract, 0.01% adenine, 0.02% tryptophan); synthetic complete (SC: 0.17% YNB, 0.2% amino acids, 0.5% ammonium sulfate); or nitrogen-limited (0.17% YNB, 0.4% proline, supplemented with histidine, leucine, methionine and uracil to complement auxotrophies as needed). Prototrophic *S. boulardii* strains were grown in SC or nitrogen-limited (0.17% YNB, 0.4% proline) without amino acid supplements. To delete *NRS1* in *S. boulardii*, the strain MYA-796 was transformed with pGZ110-Cas9-amd-SYM-nrs1_sgRNA and plated on acetamide-containing medium. Deletion alleles were confirmed by DNA sequencing of the coding region and the pGZ110 plasmid was counterselected on fluoroacetamide medium [92]. Carbon sources were added to 2% w/v as indicated. Unless otherwise specified, cells were grown to saturation in SC + 2% glucose and diluted 1 in

5,000 into fresh medium for 16 to 18 hours growth prior to experiments. These conditions ensured homeostatic growth in log-phase at the time of experiment at a culture density of 2 to $5\,10^6$ cells/mL. For strains bearing constructs expressed under the inducible *GAL1* promoter, pre-growth was in SC + 2% raffinose. Cell size distributions were acquired using a Beckman Coulter Z2 counter (Beckman Coulter, Brea, CA, USA). Growth curves were acquired at 30° C using a Tecan Sunrise shaker-reader (Tecan Group Ltd., Männedorf, Switzerland).

SGA screen

A $cln3\Delta$ $bck2\Delta$ whi5::GAL1-WHI5 strain was mated to an array of 5,280 GAL1-ORF fusion strains [41]. Following haploid selection, strains were scored for growth on selective medium containing 2% galactose. Three replicates of this screen were performed. For the third replicate, expression of the GAL4 transcription factor was increased in case it was limiting for expression of WHI5, the ORFs, or GAL genes required for growth in the presence of galactose at the sole carbon source. For this purpose, GAL4 was placed under the control of the ADH1 promoter in a cln3::LEU2 $bck2::NAT^R$ $whi5::Kan^R$ -pGAL1-WHI5 can1d mfa1::MFA1pr-spHIS5 + GAL4p::HphRpADH1-GAL4 query strain. Screen hits were validated by transformation of the GAL1-GST-ORF construct directly into the $cln3\Delta$ $bck2\Delta$ whi5::GAL1-WHI5 query strain.

Chromatin immunoprecipitation

Cells were grown in XY with 2% raffinose, induced with 2% galactose for 6 hours to an $OD_{600} \le 0.5$ and fixed with 1% formaldehyde. Whole-cell extracts from 50 mL of culture were prepared by glass bead lysis, sonicated to shear chromatin DNA into fragments, and incubated with the appropriate antibody coupled to magnetic beads (Dynabeads PanMouse IgG). Immunoprecipitated DNA was washed, de-crosslinked, purified, and analyzed by quantitative real-time PCR. Reactions with appropriate oligonucleotides were set-up with SYBR Green PCR Master Mix (Applied Biosystems, Waltham, Massachusetts, USA) and carried out on an ABI 7500 Fast Real-Time PCR System. Enrichment at the *CLN2* or *PCL1* locus was determined after normalization against values obtained from input samples using *SYP1* as the reference gene. HAWhi5 and Nrs1 $^{13\text{MYC}}$ ChIP experiments were performed in biological duplicates. The bar height on Fig 6A and 54 A Fig represent the mean over duplicates, and the error bars represent the standard error on the mean.

Immunoprecipitation and immunoblot analysis

Protein extracts were prepared in lysis buffer (10 mM HEPES-KOH pH 7.9, 50 mM KCl, 1.5 mM MgCl₂, 1 mm EDTA, 0.5 mM DTT, 50 mM NaF, 50 mM sodium pyrophosphate, 1 mM Na₃VO₄ and Roche protease inhibitor cocktail; Roche, Basel, Switzerland) by glass bead lysis. On S3C Fig, the lysis buffer contained 200mM NaCl, 50 mM HEPES pH 7.5, 1 mM EDTA, 1 mM DTT, 1.5 mM MgCl₂, protease inhibitors, 2 mM NaF, and 2 mM Na-pyrophosphate. Due to low expression levels in the 60 to 150 nM range (Fig 2D and [22]), in some cases, we concentrated Nrs1^{13MYC} by immunoprecipitation prior to immunoblot detection. Immunoprecipitations were carried out at 4°C for 2 hours with indicated antibodies in soluble form (9E10 anti-MYC from EMD Millipore, Burlington, Massachusetts, USA, 05–419; M2 anti-FLAG from Sigma, St Louis, Missouri, USA, F1804) then bound to protein G resin (Pierce, Waltham, Massachusetts, USA, 20398) for 1 hour at 4°C, followed by either 1 or 3 washes with wash buffer (10 mM Tris-Cl pH7.9, 0.1% Triton X-100, 0.5 mM DTT, 0.2 mM EDTA, 10% glycerol, 150 mM NaCl; for Fig 5A, Wash buffer: 10 mM Tris-HCl pH7.9, 0.5 mM DTT, 0.2 mM EDTA, 150 mM NaCl), and resuspension in SDS sample buffer. In Fig 5A, the immunoprecipitations were performed as above except that cell pellets were resuspended in 200 mM NaCl, 50 mM

HEPES-KOH pH 7.9, 5mM EDTA, 1 mM DTT, MCE protease inhibitors, 2 mM NaF, 2 mM Na-pyrophosphate, 0.1% NP-40 prior to lysis and complexes captured directly onto 15 μL of M2 anti-FLAG resin (anti-FLAG M2 affinity gel Sigma, A2220). For S3C Fig, the complexes were captured directly onto 15 μL of anti-MYC resin (Pierce, 20168). Proteins were resolved by SDS-PAGE, transferred onto nitrocellulose membrane, and immunoblotted with anti-HA, anti-Swi4 (gift from Brenda Andrews), anti-Swi6 (gift from Kim Nasmyth), anti-GST, anti-MYC 9E10, or anti-FLAG M2 antibodies, followed by detection with the appropriate HRP-conjugated secondary antibody [12,93].

In vitro binding assays

Recombinant GST-Nrs1 fusion protein was affinity purified with GSH-Sepharose 4B (Amersham Biosciences, Little Chalfont, Buckinghamshire, UK) in 50 mM HEPES-NaOH, pH 7.5, 150 mM NaCl, 5 mM EDTA, 5 mM NaF, 0.1% NP-40, 10% glycerol, supplemented with 1 mM PMSF. Recombinant SBF or MBF complex was purified with anti-FLAG resin (M2, Sigma) from insect cells co-infected with FLAGSwi4-Swi6 or FLAGMbp1-Swi6 baculovirus constructs in buffer supplemented with complete protease inhibitor cocktail (Roche) and then eluted with excess FLAG peptide [12]. Binding reactions were incubated at 4°C for 1 hour with rotation. Washed samples were resolved on SDS-PAGE gel followed by immunoblotting with anti-FLAG (M2, Sigma) and anti-Swi6. SBF-GST-Nrs1 and SBF-HA-Whi5 complexes were preformed in solution and immobilized on glutathione or anti-HA resin, respectively, incubated with GST-Nrs1 or HAWhi5, washed and analyzed as described above.

Immunoprecipitation and mass spectrometry analysis

Cell pellets from untagged and Nrs1 $^{13\text{MYC}}$ strains from 100 mL of culture at OD₆₀₀ = 1 were lysed in standard lysis buffer (50 mM Tris-HCl pH8.0, 150 mM KCl, 100 mM NaF, 10% glycerol, 0.1% tween-20, 1 mM tungstate, 1 mM DTT, 10 mM AEBSF, 10 mM pepstatin A, 10 mM E-64) [56] supplemented with protease inhibitors using a N₂(l) freezer mill. Lysates (0.5 mL) were incubated for 1 hour with 5 μL of anti-MYC antibody (Gentex, Zeeland, MI, USA) followed by 1-hour incubation with an additional 50 µL of GammaBind plus Sepharose beads (GE Healthcare, Chicago, IL, USA) to capture protein complexes. After multiple washes, samples were separated on Bio-Rad (Hercules, CA, USA) precast gels, and the entire gel lane was cut for each sample (CAPCA core facility, https://capca.iric.ca; see Supporting information Methods). Gel samples were destained, alkylated, and digested with trypsin for 8 hours at 37°C and peptides extracted in 90% ACN. Peptides were separated on a home-made C18 column connected to Q-Exactive HF Biopharma with a 56-minute gradient of 0% to 30% acetonitrile in 0.2% formic acid. Each full MS spectrum of extracted peptides was acquired at a resolution of 120,000, followed by acquisition of 15 tandem MS (MS-MS) spectra on the most abundant multiply charged precursor ions by collision-induced dissociation (HCD). Data were processed using PEAKS X (Bioinformatics Solutions, Waterloo, Ontario, Canada) and the Uni-Prot yeast database. Variable selected posttranslational modifications were carbamidomethyl (C), oxidation (M), deamidation (NQ), acetyl (N-ter), and phosphorylation (STY). Control untagged and Nrs1^{13MYC} data were analyzed with Scaffold 4.8.9 at an FDR of 1% for at least 2 peptides with a likelihood of at least 99%.

RNA-seq analysis

Wild-type and *GAL1-NRS1* strains were inoculated for overnight growth in SC + 2% raffinose at 30°C, then diluted in SC + 2% raffinose to an OD600 of 0.07–0.1, incubated at 30°C until an OD600 of 0.15–0.2 was reached, at which point a sample was collected for RNA extraction

prior to galactose induction. For *NRS1* induction, the cultures were either concentrated by centrifugation, resuspended in 20 mL SC+2% raffinose and added to 200 mL SC+2% galactose (replicate 2,3) or grown to an OD600 of 0.15 to 0.2 in 200 mL SC + 2% raffinose followed direct addition of 2% galactose to the culture (replicate 1). Time point 0 was collected immediately, followed by time points up to 6 hours. Total RNA was prepared as described in [94]. Briefly, cells were pelleted at 3500 rpm, disrupted using glass beads, phenol/chloroform extracted, and the aqueous phase containing nucleic acids was ethanol-precipitated. Contaminating genomic DNA was removed by DNase treatment (Qiagen, Hilden, Germany). Total RNA was quantified using Qubit (Thermo Scientific, Waltham, MA, USA) and RNA quality assessed with a 2100 Bioanalyzer (Agilent Technologies, Santa Clara, CA, USA). Transcriptome libraries were generated using the Kapa RNA HyperPrep (Roche) using a Poly-A selection (Thermo Scientific). Sequencing was performed on the Illumina NextSeq 500 system, aiming for 10 million single-end reads per sample, 40 million for raffinose, and final (6 hours) induced time points. RNA-seq experiments were performed in biological triplicate.

Reads were aligned to all Ensembl yeast transcripts using Bowtie 2.2.5 [95] with default parameters. Read counts were tabulated for each gene, only considering alignments with an edit distance no greater than 5. Genes with at least 500 reads in at least 1 sample were included in the analysis. Gene expression levels for each sample, expressed as log2 read counts, were normalized to the upper quartile gene expression level for the same sample, as recommended in Bullard and colleagues [96], and represented as heatmaps Fig 6C.

For each of the 3 GAL1-NRS1 biological replicate samples, the expression after 6 hours galactose induction was normalized separately to the expression in raffinose (prior to induction) and to the wild-type sample from the same replicate after 6 hours induction. The former controls for the sample-to-sample variation, while the latter controls for the effect of the switch to galactose-containing media. To ensure to the best possible extent that observed expression differences are due to NRS1 expression and not to one of the 2 abovementioned sources of variation, the direction and magnitude of the differential expression of each gene had to be reproduced relative to both controls. We thus kept as the final score for each replicate the smallest absolute log2-fold change produced by either of the 2 comparisons and set the score to zero if the signs of the 2 disagreed. The values for each of the 3 replicates were averaged to yield the final gene score (S6 Table). This procedure was designed to control for the effects of galactose medium (i.e., normalizing by 6 hours wild-type samples) and for intersample expression variability (i.e., normalization to expression levels prior to induction of each culture and averaging over replicates). Hence, high scores for GAL1-NRS1 (positive or negative) could be obtained only for genes up-/down-regulated both in galactose compared to raffinose and compared to wild-type cells in galactose. Wild-type 6 hours scores (S6 Table) were obtained in the same fashion except that gene expression in wild-type cells after 6 hours in galactose were normalized separately to wild-type expression in raffinose and to GAL1-NRS1 after 6-hour induction. This control analysis is symmetrical and thus equivalent to the analysis performed on GAL-NRS1 samples.

High-content imaging

High-content images were acquired on an OPERA high-throughput confocal microscope (PerkinElmer, Waltham, MA, USA) equipped with a $60\times$ water objective. Pixel resolution was 220 nm at 2^*2 binning. 200 μ L of culture were directly transferred to a Greiner Screenstar glass-bottom 96-well imaging plate and imaged within 30 to 45 minutes. GFP was excited with a 488 nm laser (800 ms exposure for endogenously tagged proteins and 320 ms for overexpressed proteins) and detected using a 520/35 nm band-pass filter. For *WHI5-GFP* and

WHI5-NRS1-GFP strains, pre-Start G1 phase cells were identified by nuclear localization of the GFP signal, as computed using a custom image-analysis script written in MATLAB (Math-Works, Natick, MA, USA). The script masks individual cells using threshold-based detection of the autofluorescence background and determines the fraction of individual cells that display a pre-Start nuclear localization of the GFP signal.

sN&B and RICS fluorescence fluctuation microscopy

Live cells in log-phase were imaged on an Alba sN&B system (ISS, Champaign Illinois, USA) comprised of an inverted confocal Nikon Eclipse microscope equipped with a 100× water objective, a Fianium Whitelase continuous white laser with 488 nm emission filters and single photon APD detectors, as described previously [22]. In brief, 1.5 mL of cell culture was pelleted for 2 minutes at 3,000 rpm in a microfuge, resuspended in approximately 100 μL of culture supernatant and 3 μL deposited on a preset 65 μL drop of SC + 2% glucose + 2% agar gel medium on a circular glass coverslip (#1, VWR) that was encircled by an adhesive silicon ring. After 4 minutes drying time, a ConcanavalinA-coated (Sigma, 2 mg/mL) coverslip was gently pressed on top of the agarose to seal the pad against the adhesive silicon ring. Sealed pads were clamped in an AttoFluor chamber (Molecular Probes, Eugene, OR, USA) and immediately imaged for no more than 1.5 hours. Unless otherwise specified, the culture growth medium was reused to make the imaging pads in order to prevent inadvertent nutrient up- or downshifts. For this purpose, 1 mL of cell culture was pelleted at 15,000 rpm for 1 minute, and 500 µL of the supernatant was mixed with 10 mg of agarose and warmed for 1 to 2 minutes at 98°C to melt the agar, followed by application to a coverslip. For sN&B experiments in the presence of rapamycin, growth medium containing 100 nM rapamycin was also used to prepare the pad. To mitigate possible degradation of rapamycin during the pad preparation, an additional 100 nM of rapamycin was added to the pre-warmed agar mix just before making the pad. The final rapamycin concentration was therefore 200 nM, i.e., about 200 ng/mL, similar to rapamycin treatment time courses in Figs 5B and S1C, and the fixed-duration treatment in Fig 5A. Cells were pretreated 1 hour before imaging and imaging lasted about 1.5 hours, yielding a treatment duration between 1 hour and 2.5 hours across the various fields of view (FOVs). There were no significant differences in Nrs1-GFP signals across different FOVs.

sN&B imaging was performed using 20 raster scans of the same 30 μ m-wide FOVs of 256 pixels (pixel size 117 nm), using an excitation power of 1 to 2 μ W at 488 nm wavelength and a 64 μ s pixel dwell time. sN&B images shown in the figures are projections of the 20 raster scans. Protein concentrations were extracted from sN&B data using custom analysis software [22]. RICS imaging was performed in a similar fashion to sN&B imaging but different parameters were used to improve correlation curves (pixel size of 48.8 nm, 50 frames, 20 μ s pixel dwell time) as described previously [56]. RICS vertical correlations for individual FOVs were fitted to single mode–free diffusion models using the SimFCS analysis software. FOVs of poor-quality fit were discarded from diffusion coefficients plots.

Bioinformatics

The sequences of orthologs of *YLR053c* were obtained from the Fungal Orthogroups website. For *Saccharomyces paradoxus* and *Saccharomyces mikatae*, where no ORF was predicted at the expected locus, the *YLR053c* sequence was searched against whole genome assemblies using TBLASTN 2.2.27 to predict orthologs. The synteny of the regions in *K. waltii* and *S. cerevisae* was confirmed based on Orthogroups orthology assignments of the upstream (47.17997 and *IES3*) and downstream (47.18006 and *OSW2*) genes and the fact that each of these assignments

were supported by highly significant Blast e-values. Alignments were generated using ClustalO 1.2.0 and displayed using the MView online tool.

Mathematical model of Start

Whisker and box plots for model predictions of the critical size at Start were obtained using the mathematical model and the data processing procedure described previously [22]. For each plot, 50 individual cells bearing variable Whi5 concentrations randomly picked in the 100 to 140 nM (for the *WHI5-GFP* strain) and 65 to 105 nM (for the *WHI5-NRS1-GFP* strain) ranges were simulated and plots generated in Excel using standard statistics of the distributions of critical size values for each strain.

Supporting information

S1 Fig. Additional characterization of Nrs1. (A) Full Ylr053c/Nrs1 protein sequence is conserved across the Saccharomyces sensu stricto group of species. Sequence alignment showing the Ylr053c/Nrs1 protein sequence in S. cerevisiae (top), aligned with sequences of orthologs in S. bayanus (c672-g32.1), S. castellii (656.13d), S. paradoxus, and S. mikatae from top to bottom. Ylr053c/Nrs1 orthologs were not predicted in S. paradoxus or S. mikatae because of sharp length cutoffs in ORF prediction algorithms (the ORFs would span only 108 and 75 residues in S. paradoxus and S. mikatae, respectively). The lack of an obvious TATA box could also explain why no protein was predicted in S. paradoxus. Neighboring upstream and downstream genes both show high similarity to YLR053c neighbors in S. cerevisiae. The YLR053c/ NRS1 sequence also aligns in S. kudriavzevii (not shown). (B) Kinetics of Nrs1 expression upon nitrogen starvation. sN&B images of untagged WT and NRS1-GFP log-phase cells (OD = 0.4 to 0.7), following 22 hours growth in YNB Pro medium from 1/5,000 dilution (left) and 7 hours growth from 1/100 dilution (right) from saturated precultures. Arrows indicate representative Nrs1 signal beyond autofluorescence at 22 hours. (C) Prolonged exposure to rapamycin results in accumulation of a faster migrating form of Nrs1. Rapamycin was added to log-phase cultures of NRS1^{13MYC} cells, aliquots were removed at indicated time intervals, and immunoprecipitates were analyzed by anti-MYC immunoblot. A raw image of the original immunoblot is provided in the S1 Raw Images. (D) Nuclear localization of Nrs1 upon rapamycin treatment is not a consequence of the particular GFPmut3 fluorophore. Confocal microscopy image of $NRS1^{WT\text{-}GFP}$ cells grown in SC + 2% glucose medium, either untreated or treated with 200 ng/mL rapamycin for 2 hours. (E) sN&B images of untagged WT cells and NRS1-GFP cells grown to log-phase in SC + 2% glucose and plated on SC + 2% glucose agar pads containing either 0.5 M NaCl or 1 mM H₂O₂ and imaged over a 2-hour time course. Images were acquired after approximately 1-hour treatment, but Nrs1 expression was not observed at any time point for any of the treatments. (F) Nrs1 is not induced by DNA damage. NRS1^{13MYC} cells grown in rich medium were exposed 0.1% MMS for 1 hour prior to immunoprecipitation and Nrs113MYC was detected with anti-MYC 9E10 antibody. Nrs1 expression from cells exposed to 200 ng/mL rapamycin and processed in parallel served as a positive control. A raw image of the original immunoblot is provided in the S1 Raw Images. NRS1, Nitrogen-Responsive Start regulator 1; sN&B, scanning Number and Brightness; WT, wild-type. (PDF)

S2 Fig. Additional characterization of $nrs1\Delta$ strains. (A) Deletion of NRS1 does not affect growth. Optical density (vertical axis) of WT (black) and $nrs1\Delta$ (blue) strains grown in SC + 2% glucose (solid lines) or nitrogen-limited (YNB+Pro, dashed lines) medium as a function of time (horizontal axis). (B-D) Deletion of NRS1 does not affect cell size. Cell size

distributions of WT (black) and *nrs1*Δ (blue) strains grown in SC + 2% glucose (**B**, solid lines), nitrogen-limited (**B**, YNB+Pro, dashed lines), SC + 2% galactose (**C**, solid lines), SC + 2% raffinose (**C**, dotted lines), YNB + 0.4% proline + 2% galactose (**C**, YNB pro gal, dashed lines), SC + 2% glucose (**D**, solid lines), SC + 4% glucose (**D**, dotted lines) and SC + 0.1% glucose (**D**, dashed lines). (**E**) Deletion of *NRS1* does not affect competitive fitness in SC + 2% glucose and nitrogen limited (YNB+Pro) medium during growth to stationary phase. Bar charts representation of the composition of 2 mixes of competing strains (Mix1: WT transformed with mCherry plasmid (red) and *nrs1*Δ transformed with Venus plasmid (green); Mix2: WT with Venus plasmid (green), and *nrs1*Δ with mCherry plasmid (red)) as a function of time from inoculation. The percentage of each strain within the mixes shown is derived from 3 replicate cultures from the same original mixes (see <u>S1 Text Methods</u>). Error bars show the standard error on the mean. All numerical values underlying this figure may be found in <u>S2 Data</u>. *NRS1*, Nitrogen-Responsive Start regulator 1; WT, wild-type. (PDF)

S3 Fig. Additional data demonstrating the physical interaction between Nrs1 and SBF. (A) Example Swi4 and Swi6 peptide spectra detected in Nrs1 immunoprecipitates. The first of the 5 peptides identified for Swi4 (ITSPSSYNKTPR) and Swi6 (SGLRPVDFGAGTSK) are shown on top and bottom, respectively. Data were processed with Scaffold software. (B) Replicate experiment for interactions detection with endogenous level of tagged proteins (Fig 5A). Swi4^{3FLAG} or Swi6^{3FLAG} complexes were immunoprecipitated from the indicated strains grown in the presence of 200 nM rapamycin for 3 hours and interacting proteins assessed by immunoblot with the indicated antibodies. Co-immunoprecipitation of Whi5^{13MYC} with Swi4^{3FLAG} and Swi6^{3FLAG} served as a positive control. Mr markers (M) are indicated for each blot. Pgk1 served as a loading control. Asterisk indicates IgG heavy and light chains. (C) Detection of endogenous untagged Swi4 and Swi6 in Nrs1^{13MYC} immunoprecipitates. Nrs1^{13MYC} or Whi5^{13MYC} complexes were immunoprecipitated from cultures of the indicated strains that were either untreated or treated with 200 nM rapamycin for 3 hours. Interacting proteins assessed by immunoblot with the indicated antibodies. Co-immunoprecipitation of Swi4 and Swi6 with Whi5^{13MYC} served as a positive control. Double asterisk indicates Whi5¹³-MYC degradation product that migrated at a similar size as Nrs1 13MYC. Mr markers (M) are indicated for each blot. NRS1, Nitrogen-Responsive Start regulator 1; SBF, SCB-binding factor. (PDF)

S4 Fig. Additional data demonstrating lack of effect of Nrs1 on Whi5. (A) NRS1 overexpression does not inhibit Whi5 association with G1/S promoter DNA. WT or WHI5^{HA} strains carrying empty vector or a GAL1-NRS1 plasmid were grown in SC + 2% raffinose medium and induced with 2% galactose for 6 hours prior to crosslinking. Anti-HA ChIPs were assessed for the presence of CLN2 and PCL1 promoter DNA by quantitative RT-PCR. Bars indicate the mean fold-enrichment across 2 replicates, and error bars show the standard error on the mean. (B) NRS1 overexpression does not affect Whi5 protein levels. Whi5-GFP absolute concentration in single WT (blue dots) and GAL1-NRS1 (orange dots) cells first grown in SC + 2% raffinose then induced with 2% galactose for 6 hours prior to sN&B microscopy. Nuclear Whi5-GFP levels in pre-Start cells and cell-averaged levels in post-Start cells where Whi5 has been exported from the nucleus are shown. All numerical values underlying panels A and B may be found in S4 Data. (C) NRS1 overexpression does not inhibit Whi5 association with SBF. The indicated Whi5^{HA} immunoprecipitates from strains induced with galactose for 6 hours were probed for Whi5^{HA}, Swi4, or Swi6 by immunoblot. (D) Nrs1 does not compete with Whi5 for binding to SBF in vitro. The indicated amounts of recombinant HAWhi5 or GSTNrs1 was titrated into preformed FLAGSwi4-Swi6-GSTNrs1 or FLAGSwi4-Swi6-HAWhi5

complexes immobilized on anti-FLAG resin, respectively. Bound proteins were resolved by SDS-PAGE then immunoblotted (top) or stained with Coomassie Brilliant Blue (bottom). Note that added soluble ^{GST}Nrs1 or ^{HA}Whi5 saturated the respective SBF-^{HA}Whi5 and SBF-^{GST}Nrs1 complexes at the lowest input concentrations. Raw image of the original immunoblots used to made panels C and D are provided in <u>S1 Raw Images</u>. ChIP, chromatin immunoprecipitation; *NRS1*, Nitrogen-Responsive Start regulator 1; SBF, SCB-binding factor; sN&B, scanning Number and Brightness; WT, wild-type. (PDF)

S5 Fig. Additional data relevant to Nrs1-mediated transactivation and GAL1-NRS1 genetic interactions. (A) Control growth curves for transactivation assays. Reporter strains transformed with plasmids expressing either GAL4^{DBD} alone, GAL4^{DBD}-NRS1, GAL4^{DBD}-UBE2G2, or GAL4^{DBD}-NRS1^{Cter} were grown in SD-Trp medium at 30°C. (B) NRS1 overexpression does not rescue a cln1Δcln2Δcln3Δ G1 phase arrest. Left: Cultures of cln1Δcln2Δcln3Δ MET-CLN2 and $cln1\Delta cln2\Delta cln3\Delta$ MET-CLN2 + <pGAL1-NRS1> strains grown to log-phase in SC-Met +2% raffinose, then reinoculated in either SC-Met+2% raffinose, SC-Met+2% galactose, SC +Met+2% raffinose or SC+Met+2% galactose for the indicated periods of time before determination of cell size distributions on a Beckman Z2 Coulter counter. Right: bar charts showing the average number of cell divisions for cln1Δcln2Δcln3Δ MET25-CLN2 and cln1Δcln2Δcln3Δ MET25-CLN2 + <pGAL1-NRS1> strains during the 18 hour interval between the 6 hours and 24 hours time points in SC+Met+2%galactose. Bar heights represent the average of 4 different clones (N = 4); error bars represent the standard deviation. (C) Room temperature growth controls for genetic interactions of NRS1 with SWI4 and MBP1. Serial 5-fold dilutions of WT *NRS1* and *nrs1::GAL1-NRS1* strains in WT (rows 1, 2, 10), *swi4-ts* (row 3), $mbp1\Delta$ (row 4), and $mbp1\Delta swi4$ -ts (rows 5–9) backgrounds were spotted onto SC + 2% glucose, SC + 2% raffinose, and SC + 2% galactose medium and grown for 5 days at 23°C. C1-4 are 4 clones of $mbp1\Delta$ swi4-ts GAL1-NRS1. (D) Images of the same serial 5-fold dilutions of NRS1 and GAL1-NRS1 strains in WT, swi4-ts, mbp1 Δ , and mbp1 Δ swi4-ts backgrounds as in Fig 7B, spotted onto SC + 2% glucose, SC + 2% raffinose and SC + 2% galactose, but grown for an additional 2 days (i.e., 7 days total growth time at 30°C). C1 to C4 are 4 clones of mbp1∆ swi4-ts GAL1-NRS1. All numerical values underlying panels A and B may be found in S6 Data. NRS1, Nitrogen-Responsive Start regulator 1; WT, wild-type. (PDF)

S6 Fig. Additional characterization and controls for Nrs1 and Whi5 fusion proteins. (A) The Whi5-Nrs1-GFP chimeric protein is produced *in vivo* and migrates at the expected size. WHI5-GFP, NRS1-GFP, and WHI5-NRS1-GFP strains were grown in nitrogen-limited (YNB +Pro) medium and extracts immunobloted with anti-GFP antibody. A raw image of the original immunoblot is provided in S1 Raw Images. (B) A carboxyl-terminal fusion of Nrs1 to Whi5 does not affect cell cycle distribution. High-content images of WHI5-GFP and WHI5-NRS1-GFP cells grown in SC + 2% glucose were acquired on an OPERA high-throughput confocal microscope (PerkinElmer) equipped with a 60× water objective. The same intensity scale was used for both panels. Scale bar is 10 µm. The fraction of pre-Start (G1) cells was obtained using a custom MATLAB script (see Methods). (C) Fusion of a GFP tag at the Whi5 carboxyl terminus does not affect cell size. Cell size distributions of untagged WT and WHI5-GFP cells grown in SC + 2% glucose were determined on a Beckman Z2 Coulter counter. (D) Growth curves of WT, whi5∆, and WHI5-NRS1-GFP strains in SC + 2% glucose medium at 30°C. (E) WHI5 dosage has only minor effects on cell size. Cell size distributions of WT and WHI5/whi5 heterozygous diploid strains grown in SC + 2% glucose. Dotted, dashed, and solid blue lines represent 3 different WHI5/whi5 clones. (F) Predicted effects of WHI5

dosage on cell size in a mathematical model of Start. Box and whisker plots show distribution of critical cell sizes predicted by the Start model published in [22] for simulated average Whi5 concentrations of 120 nM (corresponding to *WHI5-GFP* cells, left boxplot) and 85 nM (corresponding to *WHI5-NRS1-GFP* cells, right boxplot). All numerical values underlying panels C–F may be found in <u>S7 Data</u>. *NRS1*, Nitrogen-Responsive Start regulator 1; WT, wild-type; YNB +Pro, YNB + 0.4% proline + 2% glucose. (PDF)

S7 Fig. Nrs1 function at G1/S requires the poorly conserved N-terminal region. (A) Cell size distributions of WT and WHI5-NRS1^{Cter}-GFP strains grown in SC+2% glucose determined on a Beckman Z2 Coulter counter. (B) Genotype of 10 tetrads from a $cln3\Delta$ whi5:: WHI5-NRS1^{Cter}-GFP X $bck2\Delta$ cross. For each tetrad, spore clone growth was assessed on SD-Leu (indicates cln3::LEU2), SC+NAT (indicates bck2::NAT^R), and SD-HIS (indicates whi5::WHI5-NRS1^{Cter}-GFP-HIS3). Blue boxes indicate viable $cln3\Delta$ or $bck2\Delta$ spore clones. No viable $cln3\Delta$ $bck2\Delta$ double mutant clones were recovered. All numerical values underlying panel A may be found in S7 Data. NRS1, Nitrogen-Responsive Start regulator 1; WT, wild-type. (PDF)

S1 Table. Candidate dosage suppressors of $cln3\Delta$ $bck2\Delta$ lethality. (XLSX)

S2 Table. Yeast strains and plasmids used in this study. (DOCX)

S3 Table. Proteins detected specifically in Nrs1 immunoprecipitates by mass spectrometry. NRS1, Nitrogen-Responsive Start regulator 1. (XLSX)

S4 Table. List of peptides identified in Nrs1 and control immunoprecipitates by mass spectrometry. NRS1, Nitrogen-Responsive Start regulator 1. (XLSX)

S5 Table. List of proteins identified in Nrs1 and control immunoprecipitates by mass spectrometry. NRS1, Nitrogen-Responsive Start regulator 1. (XLSX)

S6 Table. Calculated gene scores for RNA-seq experiments performed with WT and *GAL1-NRS1* strains. For up-regulated (score >0) and strongly up-regulated (score > 0.5) genes, Swi4/Mbp1-binding scores were imported from Ferrezuelo and colleagues [10], and SBF/MBF targets were identified and counted. These data were used to perform the hypergeometric enrichment tests. MBF, MCB-binding factor; *NRS1*, Nitrogen-Responsive Start regulator 1; RNA-seq, RNA sequencing; SBF, SCB-binding factor; WT, wild-type. (XLSX)

S1 Raw Images. Contains raw images of uncropped gels (western blots, Coomassie, Ponceau) used in the manuscript. (PDF)

S1 Data. Raw numerical data used to generate Fig 2D and 2E. (XLSX)

S2 Data. Raw numerical data used to generate Figs $\underline{3}$ and $\underline{S2}$. (XLSX)

S3 Data. Raw numerical data used to generate Fig 4A and 4B.

(XLSX)

S4 Data. Raw numerical data used to generate S4A and S4B Fig.

(XLSX)

S5 Data. Raw numerical data used to generate Fig 6A and 6B.

(XLSX)

S6 Data. Raw numerical data used to generate Figs 7A and S5A and S5B.

(XLSX)

S7 Data. Raw numerical data used to generate Figs <u>8A-8C</u> and <u>S6C-S6F</u> and <u>S7A</u>.

(XLSX)

S1 Text. Supporting information.

(PDF)

Acknowledgments

We thank Marc Angeli for technical assistance with SGA screens, Brenda Andrews and Kim Nasmyth for providing antibody reagents and strains, and Elizabeth Bilsland for yeast fluorescent protein vectors. We also thank Jennifer Huber of the IRIC Genomics Platform for assistance with RNA-seq experiments.

Author Contributions

Conceptualization: Sylvain Tollis, Jaspal Singh, Mike Tyers.

Data curation: Sylvain Tollis, Jasmin Coulombe-Huntington, Eric Bonneil.

Formal analysis: Sylvain Tollis, Jasmin Coulombe-Huntington, Eric Bonneil.

Funding acquisition: Sylvain Tollis, Pierre Thibault, Mike Tyers.

Investigation: Sylvain Tollis, Jaspal Singh, Roger Palou, Yogitha Thattikota, Ghada Ghazal, Xiaojing Tang, Susan Moore, Deborah Blake.

Methodology: Sylvain Tollis, Jaspal Singh, Xiaojing Tang, Susan Moore, Catherine A. Royer, Mike Tyers.

Project administration: Sylvain Tollis, Mike Tyers.

Resources: Sylvain Tollis, Jaspal Singh, Roger Palou, Yogitha Thattikota, Ghada Ghazal, Xiaojing Tang, Susan Moore, Deborah Blake.

Software: Sylvain Tollis, Jasmin Coulombe-Huntington.

Supervision: Sylvain Tollis, Mike Tyers.

Validation: Sylvain Tollis, Jaspal Singh, Roger Palou, Yogitha Thattikota, Ghada Ghazal, Xiaojing Tang, Susan Moore, Deborah Blake.

Visualization: Sylvain Tollis, Jaspal Singh, Roger Palou, Ghada Ghazal, Jasmin Coulombe-Huntington, Eric Bonneil.

Writing - original draft: Sylvain Tollis, Jaspal Singh, Deborah Blake, Eric Bonneil.

Writing – review & editing: Sylvain Tollis, Roger Palou, Yogitha Thattikota, Ghada Ghazal, Jasmin Coulombe-Huntington, Catherine A. Royer, Pierre Thibault, Mike Tyers.

References

- Broach JR. Nutritional control of growth and development in yeast. Genetics. 2012; 192(1):73–105. https://doi.org/10.1534/genetics.111.135731 PMID: 22964838
- Johnston GC, Pringle JR, Hartwell LH. Coordination of growth with cell division in the yeast Saccharomyces cerevisiae. Exp Cell Res. 1977; 105(1):79–98. https://doi.org/10.1016/0014-4827(77)90154-9 PMID: 320023
- Jorgensen P, Tyers M. How cells coordinate growth and division. Curr Biol. 2004; 14(23):R1014–27. https://doi.org/10.1016/j.cub.2004.11.027 PMID: 15589139
- Lowndes NF, Johnson AL, Breeden L, Johnston LH. SWI6 protein is required for transcription of the periodically expressed DNA synthesis genes in budding yeast. Nature. 1992; 357(6378):505–8. https://doi.org/10.1038/357505a0 PMID: 1608450
- Primig M, Sockanathan S, Auer H, Nasmyth K. Anatomy of a transcription factor important for the start of the cell cycle in Saccharomyces cerevisiae. Nature. 1992; 358(6387):593–7. https://doi.org/10.1038/358593a0 PMID: 1386897
- Koch C, Moll T, Neuberg M, Ahorn H, Nasmyth K. A role for the transcription factors Mbp1 and Swi4 in progression from G1 to S phase. Science. 1993; 261(5128):1551–7. https://doi.org/10.1126/science.8372350 PMID: 8372350
- Iyer VR, Horak CE, Scafe CS, Botstein D, Snyder M, Brown PO. Genomic binding sites of the yeast cell-cycle transcription factors SBF and MBF. Nature. 2001; 409(6819):533–8. https://doi.org/10.1038/35054095 PMID: 11206552
- Lee TI, Rinaldi NJ, Robert F, Odom DT, Bar-Joseph Z, Gerber GK, et al. Transcriptional regulatory networks in Saccharomyces cerevisiae. Science. 2002; 298(5594):799–804. https://doi.org/10.1126/science.1075090 PMID: 12399584
- Simon I, Barnett J, Hannett N, Harbison CT, Rinaldi NJ, Volkert TL, et al. Serial regulation of transcriptional regulators in the yeast cell cycle. Cell. 2001; 106(6):697–708. https://doi.org/10.1016/s0092-8674 (01)00494-9 PMID: 11572776
- Ferrezuelo F, Colomina N, Futcher B, Aldea M. The transcriptional network activated by Cln3 cyclin at the G1-to-S transition of the yeast cell cycle. Genome Biol. 2010; 11(6):R67. https://doi.org/10.1186/gb-2010-11-6-r67 PMID: 20573214
- Jorgensen P, Nishikawa JL, Breitkreutz BJ, Tyers M. Systematic identification of pathways that couple cell growth and division in yeast. Science. 2002; 297(5580):395–400. https://doi.org/10.1126/science.1070850 PMID: 12089449
- Costanzo M, Nishikawa JL, Tang X, Millman JS, Schub O, Breitkreuz K, et al. CDK activity antagonizes Whi5, an inhibitor of G1/S transcription in yeast. Cell. 2004; 117(7):899–913. https://doi.org/10.1016/j.cell.2004.05.024 PMID: 15210111
- 13. de Bruin RA, McDonald WH, Kalashnikova TI, Yates J 3rd, Wittenberg C. Cln3 activates G1-specific transcription via phosphorylation of the SBF bound repressor Whi5. Cell. 2004; 117(7):887–98. https://doi.org/10.1016/j.cell.2004.05.025 PMID: 15210110
- 14. Wagner MV, Smolka MB, de Bruin RA, Zhou H, Wittenberg C, Dowdy SF. Whi5 regulation by site specific CDK-phosphorylation in Saccharomyces cerevisiae. PLoS ONE. 2009; 4(1):e4300. https://doi.org/10.1371/journal.pone.0004300 PMID: 19172996
- Skotheim JM, Di Talia S, Siggia ED, Cross FR. Positive feedback of G1 cyclins ensures coherent cell cycle entry. Nature. 2008; 454(7202):291–6. https://doi.org/10.1038/nature07118 PMID: 18633409
- Tyers M, Tokiwa G, Futcher B. Comparison of the Saccharomyces cerevisiae G1 cyclins: Cln3 may be an upstream activator of Cln1, Cln2 and other cyclins. EMBO J. 1993; 12(5):1955–68. PMID: 8387915
- McInerny CJ, Partridge JF, Mikesell GE, Creemer DP, Breeden LL. A novel Mcm1-dependent element in the SWI4, CLN3, CDC6, and CDC47 promoters activates M/G1-specific transcription. Genes Dev. 1997; 11(10):1277–88. https://doi.org/10.1101/gad.11.10.1277 PMID: 9171372
- Nash R, Tokiwa G, Anand S, Erickson K, Futcher AB. The WHI1+ gene of Saccharomyces cerevisiae tethers cell division to cell size and is a cyclin homolog. EMBO J. 1988; 7(13):4335–46. PMID: 2907481
- Cross FR. DAF1, a mutant gene affecting size control, pheromone arrest, and cell cycle kinetics of Saccharomyces cerevisiae. Mol Cell Biol. 1988; 8(11):4675–84. https://doi.org/10.1128/mcb.8.11.4675-4684.1988 PMID: 3062366
- Liu X, Wang X, Yang X, Liu S, Jiang L, Qu Y, et al. Reliable cell cycle commitment in budding yeast is ensured by signal integration. Elife. 2015;4. https://doi.org/10.7554/eLife.03977 PMID: 25590650

- Litsios A, Huberts D, Terpstra HM, Guerra P, Schmidt A, Buczak K, et al. Differential scaling between G1 protein production and cell size dynamics promotes commitment to the cell division cycle in budding yeast. Nat Cell Biol. 2019; 21(11):1382–92. https://doi.org/10.1038/s41556-019-0413-3 PMID: 31685990
- Dorsey S, Tollis S, Cheng J, Black L, Notley S, Tyers M, et al. G1/S Transcription Factor Copy Number Is a Growth-Dependent Determinant of Cell Cycle Commitment in Yeast. Cell Syst. 2018; 6(5):539–54 e11. https://doi.org/10.1016/j.cels.2018.04.012 PMID: 29792825
- Schmoller KM, Turner JJ, Koivomagi M, Skotheim JM. Dilution of the cell cycle inhibitor Whi5 controls budding-yeast cell size. Nature. 2015; 526(7572):268–72. https://doi.org/10.1038/nature14908 PMID: 26390151
- 24. Barber F, Amir A, Murray AW. Cell-size regulation in budding yeast does not depend on linear accumulation of Whi5. Proc Natl Acad Sci U S A. 2020; 117(25):14243–50. https://doi.org/10.1073/pnas.2001255117 PMID: 32518113
- Sommer RA, DeWitt JT, Tan R, Kellogg DR. Growth-dependent signals drive an increase in early G1 cyclin concentration to link cell cycle entry with cell growth. Elife. 2021;10. https://doi.org/10.7554/eLife.64364 PMID: 34713806
- Black L, Tollis S, Fu G, Fiche JB, Dorsey S, Cheng J, et al. G1/S transcription factors assemble in increasing numbers of discrete clusters through G1 phase. J Cell Biol. 2020; 219(9). https://doi.org/10.1083/icb.202003041 PMID: 32744610
- 27. Chen Y, Zhao G, Zahumensky J, Honey S, Futcher B. Differential Scaling of Gene Expression with Cell Size May Explain Size Control in Budding Yeast. Mol Cell. 2020; 78(2):359–70 e6. https://doi.org/10.1016/j.molcel.2020.03.012 PMID: 32246903
- Koivomagi M, Swaffer MP, Turner JJ, Marinov G, Skotheim JM. G1 cyclin-Cdk promotes cell cycle entry through localized phosphorylation of RNA polymerase II. Science. 2021; 374(6565):347–51. https://doi.org/10.1126/science.aba5186 PMID: 34648313
- Wijnen H, Futcher B. Genetic analysis of the shared role of CLN3 and BCK2 at the G(1)-S transition in Saccharomyces cerevisiae. Genetics. 1999; 153(3):1131–43. https://doi.org/10.1093/genetics/153.3.1131 PMID: 10545447
- Bastajian N, Friesen H, Andrews BJ. Bck2 acts through the MADS box protein Mcm1 to activate cell-cycle-regulated genes in budding yeast. PLoS Genet. 2013; 9(5):e1003507. https://doi.org/10.1371/journal.pgen.1003507 PMID: 23675312
- Tokiwa G, Tyers M, Volpe T, Futcher B. Inhibition of G1 cyclin activity by the Ras/cAMP pathway in yeast. Nature. 1994; 371(6495):342–5. https://doi.org/10.1038/371342a0 PMID: 8090204
- Flick K, Chapman-Shimshoni D, Stuart D, Guaderrama M, Wittenberg C. Regulation of cell size by glucose is exerted via repression of the CLN1 promoter. Mol Cell Biol. 1998; 18(5):2492–501. https://doi.org/10.1128/MCB.18.5.2492 PMID: 9566870
- Jorgensen P, Rupes I, Sharom JR, Schneper L, Broach JR, Tyers M. A dynamic transcriptional network communicates growth potential to ribosome synthesis and critical cell size. Genes Dev. 2004; 18 (20):2491–505. https://doi.org/10.1101/gad.1228804 PMID: 15466158
- 34. Lempiainen H, Uotila A, Urban J, Dohnal I, Ammerer G, Loewith R, et al. Sfp1 interaction with TORC1 and Mrs6 reveals feedback regulation on TOR signaling. Mol Cell. 2009; 33(6):704–16. https://doi.org/10.1016/j.molcel.2009.01.034 PMID: 19328065
- Singh J, Tyers M. A Rab escort protein integrates the secretion system with TOR signaling and ribosome biogenesis. Genes Dev. 2009; 23(16):1944–58. https://doi.org/10.1101/gad.1804409 PMID: 19684114
- Urban J, Soulard A, Huber A, Lippman S, Mukhopadhyay D, Deloche O, et al. Sch9 is a major target of TORC1 in Saccharomyces cerevisiae. Mol Cell. 2007; 26(5):663–74. https://doi.org/10.1016/j.molcel.2007.04.020 PMID: 17560372
- 37. Talarek N, Gueydon E, Schwob E. Homeostatic control of START through negative feedback between Cln3-Cdk1 and Rim15/Greatwall kinase in budding yeast. Elife. 2017;6. https://doi.org/10.7554/eLife.26233 PMID: 28600888
- 38. Epstein CB, Cross FR. Genes that can bypass the CLN requirement for Saccharomyces cerevisiae cell cycle START. Mol Cell Biol. 1994; 14(3):2041–7. https://doi.org/10.1128/mcb.14.3.2041-2047.1994 PMID: 8114735
- Di Como CJ, Chang H, Arndt KT. Activation of CLN1 and CLN2 G1 cyclin gene expression by BCK2.
 Mol Cell Biol. 1995; 15(4):1835–46. https://doi.org/10.1128/MCB.15.4.1835 PMID: 7891677
- Tong AH, Evangelista M, Parsons AB, Xu H, Bader GD, Page N, et al. Systematic genetic analysis with ordered arrays of yeast deletion mutants. Science. 2001; 294(5550):2364–8. https://doi.org/10.1126/science.1065810 PMID: 11743205

- Sopko R, Huang D, Preston N, Chua G, Papp B, Kafadar K, et al. Mapping pathways and phenotypes by systematic gene overexpression. Mol Cell. 2006; 21(3):319–30. https://doi.org/10.1016/j.molcel.2005.12.011 PMID: 16455487
- Zhu H, Bilgin M, Bangham R, Hall D, Casamayor A, Bertone P, et al. Global analysis of protein activities using proteome chips. Science. 2001; 293(5537):2101–5. https://doi.org/10.1126/science.1062191 PMID: 11474067
- Carvunis AR, Rolland T, Wapinski I, Calderwood MA, Yildirim MA, Simonis N, et al. Proto-genes and de novo gene birth. Nature. 2012; 487(7407):370–4. https://doi.org/10.1038/nature11184 PMID: 22722833
- Digman MA, Dalal R, Horwitz AF, Gratton E. Mapping the number of molecules and brightness in the laser scanning microscope. Biophys J. 2008; 94(6):2320–32. https://doi.org/10.1529/biophysj.107.114645 PMID: 18096627
- Balleza E, Kim JM, Cluzel P. Systematic characterization of maturation time of fluorescent proteins in living cells. Nat Methods. 2018; 15(1):47–51. https://doi.org/10.1038/nmeth.4509 PMID: 29320486
- 46. Daran-Lapujade P, Jansen ML, Daran JM, van Gulik W, de Winde JH, Pronk JT. Role of transcriptional regulation in controlling fluxes in central carbon metabolism of Saccharomyces cerevisiae. A chemostat culture study. J Biol Chem. 2004; 279(10):9125–38. https://doi.org/10.1074/jbc.M309578200 PMID: 14630934
- Boer VM, de Winde JH, Pronk JT, Piper MD. The genome-wide transcriptional responses of Saccharomyces cerevisiae grown on glucose in aerobic chemostat cultures limited for carbon, nitrogen, phosphorus, or sulfur. J Biol Chem. 2003; 278(5):3265–74. https://doi.org/10.1074/jbc.M209759200 PMID: 12414795
- Blinder D, Magasanik B. Recognition of nitrogen-responsive upstream activation sequences of Saccharomyces cerevisiae by the product of the GLN3 gene. J Bacteriol. 1995; 177(14):4190–3. https://doi.org/10.1128/jb.177.14.4190-4193.1995 PMID: 7608102
- 49. de Boer CG, Hughes TR. YeTFaSCo: a database of evaluated yeast transcription factor sequence specificities. Nucleic Acids Res. 2012; 40(Database issue):D169–79. https://doi.org/10.1093/nar/gkr993 PMID: 22102575
- Gelperin DM, White MA, Wilkinson ML, Kon Y, Kung LA, Wise KJ, et al. Biochemical and genetic analysis of the yeast proteome with a movable ORF collection. Genes Dev. 2005; 19(23):2816–26. https://doi.org/10.1101/gad.1362105 PMID: 16322557
- Ogas J, Andrews BJ, Herskowitz I. Transcriptional activation of CLN1, CLN2, and a putative new G1 cyclin (HCS26) by SWI4, a positive regulator of G1-specific transcription. Cell. 1991; 66(5):1015–26. https://doi.org/10.1016/0092-8674(91)90445-5 PMID: 1832336
- Khatri I, Tomar R, Ganesan K, Prasad GS, Subramanian S. Complete genome sequence and comparative genomics of the probiotic yeast Saccharomyces boulardii. Sci Rep. 2017; 7(1):371. https://doi.org/10.1038/s41598-017-00414-2 PMID: 28336969
- Mellacheruvu D, Wright Z, Couzens AL, Lambert JP, St-Denis NA, Li T, et al. The CRAPome: a contaminant repository for affinity purification-mass spectrometry data. Nat Methods. 2013; 10(8):730–6. https://doi.org/10.1038/nmeth.2557 PMID: 23921808
- 54. Brown CM, Dalal RB, Hebert B, Digman MA, Horwitz AR, Gratton E. Raster image correlation spectroscopy (RICS) for measuring fast protein dynamics and concentrations with a commercial laser scanning confocal microscope. J Microsc. 2008; 229(Pt 1):78–91. https://doi.org/10.1111/j.1365-2818.2007.
 01871.x PMID: 18173647
- Digman MA, Wiseman PW, Horwitz AR, Gratton E. Detecting protein complexes in living cells from laser scanning confocal image sequences by the cross correlation raster image spectroscopy method. Biophys J. 2009; 96(2):707–16. https://doi.org/10.1016/j.bpj.2008.09.051 PMID: 19167315
- 56. Thattikota Y, Tollis S, Palou R, Vinet J, Tyers M. D'Amours D. Cdc48/VCP Promotes Chromosome Morphogenesis by Releasing Condensin from Self-Entrapment in Chromatin. Mol Cell. 2018; 69(4):664–76 e5. https://doi.org/10.1016/j.molcel.2018.01.030 PMID: 29452641
- 57. Bean JM, Siggia ED, Cross FR. High functional overlap between Mlul cell-cycle box binding factor and Swi4/6 cell-cycle box binding factor in the G1/S transcriptional program in Saccharomyces cerevisiae. Genetics. 2005; 171(1):49–61. https://doi.org/10.1534/genetics.105.044560 PMID: https://doi.org/10.1534/genetics.105.044560 PMID: https://doi.org/10.1534/genetics.105.044560
- 58. Gray JV, Ogas JP, Kamada Y, Stone M, Levin DE, Herskowitz I. A role for the Pkc1 MAP kinase pathway of Saccharomyces cerevisiae in bud emergence and identification of a putative upstream regulator. EMBO J. 1997; 16(16):4924–37. https://doi.org/10.1093/emboj/16.16.4924 PMID: 9305635
- Adames NR, Schuck PL, Chen KC, Murali TM, Tyson JJ, Peccoud J. Experimental testing of a new integrated model of the budding yeast Start transition. Mol Biol Cell. 2015; 26(22):3966–84. https://doi.org/10.1091/mbc.E15-06-0358 PMID: 26310445

- Oughtred R, Stark C, Breitkreutz BJ, Rust J, Boucher L, Chang C, et al. The BioGRID interaction database: 2019 update. Nucleic Acids Res. 2019; 47(D1):D529–D41. https://doi.org/10.1093/nar/gky1079
 PMID: 30476227
- Atencio D, Barnes C, Duncan TM, Willis IM, Hanes SD. The yeast Ess1 prolyl isomerase controls Swi6 and Whi5 nuclear localization. G3 (Bethesda). 2014; 4(3):523–37. https://doi.org/10.1534/g3.113.
 008763 PMID: 24470217
- Sharifpoor S, van Dyk D, Costanzo M, Baryshnikova A, Friesen H, Douglas AC, et al. Functional wiring
 of the yeast kinome revealed by global analysis of genetic network motifs. Genome Res. 2012; 22
 (4):791–801. https://doi.org/10.1101/gr.129213.111 PMID: 22282571
- 63. Costanzo M, VanderSluis B, Koch EN, Baryshnikova A, Pons C, Tan G, et al. A global genetic interaction network maps a wiring diagram of cellular function. Science. 2016; 353(6306). https://doi.org/10.1126/science.aaf1420 PMID: 27708008
- 64. Frumkin JP, Patra BN, Sevold A, Ganguly K, Patel C, Yoon S, et al. The interplay between chromosome stability and cell cycle control explored through gene-gene interaction and computational simulation. Nucleic Acids Res. 2016; 44(17):8073–85. https://doi.org/10.1093/nar/gkw715 PMID: 27530428
- 65. Tanaka S, Diffley JF. Deregulated G1-cyclin expression induces genomic instability by preventing efficient pre-RC formation. Genes Dev. 2002; 16(20):2639–49. https://doi.org/10.1101/gad.1011002 PMID: 12381663
- 66. Ma J, Ward CC, Jungreis I, Slavoff SA, Schwaid AG, Neveu J, et al. Discovery of human sORF-encoded polypeptides (SEPs) in cell lines and tissue. J Proteome Res. 2014; 13(3):1757–65. https://doi.org/10.1021/pr401280w PMID: 24490786
- Ladoukakis E, Pereira V, Magny EG, Eyre-Walker A, Couso JP. Hundreds of putatively functional small open reading frames in Drosophila. Genome Biol. 2011; 12(11):R118. https://doi.org/10.1186/gb-2011-12-11-r118 PMID: 22118156
- 68. Kastenmayer JP, Ni L, Chu A, Kitchen LE, Au WC, Yang H, et al. Functional genomics of genes with small open reading frames (sORFs) in S. cerevisiae. Genome Res. 2006; 16(3):365–73. https://doi.org/10.1101/gr.4355406 PMID: 16510898
- 69. Ma J, Diedrich JK, Jungreis I, Donaldson C, Vaughan J, Kellis M, et al. Improved Identification and Analysis of Small Open Reading Frame Encoded Polypeptides. Anal Chem. 2016; 88(7):3967–75. https://doi.org/10.1021/acs.analchem.6b00191 PMID: 27010111
- Pueyo JI, Magny EG, Sampson CJ, Amin U, Evans IR, Bishop SA, et al. Hemotin, a Regulator of Phagocytosis Encoded by a Small ORF and Conserved across Metazoans. PLoS Biol. 2016; 14(3): e1002395. https://doi.org/10.1371/journal.pbio.1002395 PMID: 27015288
- Gong Z, Tasset I, Diaz A, Anguiano J, Tas E, Cui L, et al. Humanin is an endogenous activator of chaperone-mediated autophagy. J Cell Biol. 2018; 217(2):635–47. https://doi.org/10.1083/jcb.201606095
 PMID: 29187525
- Polycarpou-Schwarz M, Gross M, Mestdagh P, Schott J, Grund SE, Hildenbrand C, et al. The cancerassociated microprotein CASIMO1 controls cell proliferation and interacts with squalene epoxidase modulating lipid droplet formation. Oncogene. 2018; 37(34):4750–68. https://doi.org/10.1038/s41388-018-0281-5 PMID: 29765154
- Li JM, Li Y, Elledge SJ. Genetic analysis of the kinetochore DASH complex reveals an antagonistic relationship with the ras/protein kinase A pathway and a novel subunit required for Ask1 association. Mol Cell Biol. 2005; 25(2):767–78. https://doi.org/10.1128/MCB.25.2.767-778.2005 PMID: 15632076
- Saghatelian A, Couso JP. Discovery and characterization of smORF-encoded bioactive polypeptides. Nat Chem Biol. 2015; 11(12):909–16. https://doi.org/10.1038/nchembio.1964 PMID: 26575237
- Cardon T, Fournier I, Salzet M. Shedding Light on the Ghost Proteome. Trends Biochem Sci. 2021; 46 (3):239–50. https://doi.org/10.1016/j.tibs.2020.10.003 PMID: 33246829
- Chen J, Brunner AD, Cogan JZ, Nunez JK, Fields AP, Adamson B, et al. Pervasive functional translation of noncanonical human open reading frames. Science. 2020; 367(6482):1140–6. https://doi.org/10.1126/science.aay0262 PMID: 32139545
- 77. Prensner JR, Enache OM, Luria V, Krug K, Clauser KR, Dempster JM, et al. Noncanonical open reading frames encode functional proteins essential for cancer cell survival. Nat Biotechnol. 2021; 39(6):697–704. https://doi.org/10.1038/s41587-020-00806-2 PMID: 33510483
- 78. Na Z, Luo Y, Schofield JA, Smelyansky S, Khitun A, Muthukumar S, et al. The NBDY Microprotein Regulates Cellular RNA Decapping. Biochemistry. 2020; 59(42):4131–42. https://doi.org/10.1021/acs.biochem.0c00672 PMID: 33059440
- Zanet J, Benrabah E, Li T, Pelissier-Monier A, Chanut-Delalande H, Ronsin B, et al. Pri sORF peptides induce selective proteasome-mediated protein processing. Science. 2015; 349(6254):1356–8. https://doi.org/10.1126/science.aac5677 PMID: 26383956

- 80. Hong SY, Sun B, Straub D, Blaakmeer A, Mineri L, Koch J, et al. Heterologous microProtein expression identifies LITTLE NINJA, a dominant regulator of jasmonic acid signaling. Proc Natl Acad Sci U S A. 2020; 117(42):26197–205. https://doi.org/10.1073/pnas.2005198117 PMID: 33033229
- 81. Koh M, Ahmad I, Ko Y, Zhang Y, Martinez TF, Diedrich JK, et al. A short ORF-encoded transcriptional regulator. Proc Natl Acad Sci U S A. 2021; 118(4).
- Wu Q, Kuang K, Lyu M, Zhao Y, Li Y, Li J, et al. Allosteric deactivation of PIFs and EIN3 by microproteins in light control of plant development. Proc Natl Acad Sci U S A. 2020; 117(31):18858–68. https://doi.org/10.1073/pnas.2002313117 PMID: 32694206
- 83. Dolde U, Rodrigues V, Straub D, Bhati KK, Choi S, Yang SW, et al. Synthetic MicroProteins: Versatile Tools for Posttranslational Regulation of Target Proteins. Plant Physiol. 2018; 176(4):3136–45. https://doi.org/10.1104/pp.17.01743 PMID: 29382693
- 84. Laumont CM, Vincent K, Hesnard L, Audemard E, Bonneil E, Laverdure JP, et al. Noncoding regions are the main source of targetable tumor-specific antigens. Sci Transl Med. 2018; 10(470). https://doi.org/10.1126/scitranslmed.aau5516 PMID: 30518613
- 85. Ouspenskaia T, Law T, Clauser KR, Klaeger S, Sarkizova S, Aguet F, et al. Unannotated proteins expand the MHC-I-restricted immunopeptidome in cancer. Nat Biotechnol. 2021. https://doi.org/10.1038/s41587-021-01021-3 PMID: 34663921
- 86. Palazzo AF, Koonin EV. Functional Long Non-coding RNAs Evolve from Junk Transcripts. Cell. 2020; 183(5):1151–61. https://doi.org/10.1016/j.cell.2020.09.047 PMID: 33068526
- Dhamija S, Menon MB. Non-coding transcript variants of protein-coding genes—what are they good for? RNA Biol. 2018; 15(8):1025–31. https://doi.org/10.1080/15476286.2018.1511675 PMID: 30146915
- 88. Ruiz-Orera J, Villanueva-Canas JL, Alba MM. Evolution of new proteins from translated sORFs in long non-coding RNAs. Exp Cell Res. 2020; 391(1):111940. https://doi.org/10.1016/j.yexcr.2020.111940 PMID: 32156600
- 89. Coulombe-Huntington J, Xia Y. Network Centrality Analysis in Fungi Reveals Complex Regulation of Lost and Gained Genes. PLoS ONE. 2017; 12(1):e0169459. https://doi.org/10.1371/journal.pone.0169459 PMID: 28046110
- 90. de Boer CG, Vaishnav ED, Sadeh R, Abeyta EL, Friedman N, Regev A. Deciphering eukaryotic generegulatory logic with 100 million random promoters. Nat Biotechnol. 2020; 38(1):56–65. https://doi.org/10.1038/s41587-019-0315-8 PMID: 31792407
- Fink GR. Guide to Yeast Genetics and Molecular and Cell Biology. Guthrie C, editor. San Francisco, California: Academic Press, Elsevier; 2002. p. 12.
- Solis-Escalante D, Kuijpers NG, Bongaerts N, Bolat I, Bosman L, Pronk JT, et al. amdSYM, a new dominant recyclable marker cassette for Saccharomyces cerevisiae. FEMS Yeast Res. 2013; 13(1):126–39. https://doi.org/10.1111/1567-1364.12024 PMID: 23253382
- 93. Tang X, Orlicky S, Mittag T, Csizmok V, Pawson T, Forman-Kay JD, et al. Composite low affinity interactions dictate recognition of the cyclin-dependent kinase inhibitor Sic1 by the SCFCdc4 ubiquitin ligase. Proc Natl Acad Sci U S A. 2012; 109(9):3287–92. https://doi.org/10.1073/pnas.1116455109 PMID: 22328159
- Ghazal G, Gagnon J, Jacques PE, Landry JR, Robert F, Elela SA. Yeast RNase III triggers polyadenylation-independent transcription termination. Mol Cell. 2009; 36(1):99–109. https://doi.org/10.1016/j.molcel.2009.07.029 PMID: 19818713
- 95. Langmead B, Salzberg SL. Fast gapped-read alignment with Bowtie 2. Nat Methods. 2012; 9(4):357–9. https://doi.org/10.1038/nmeth.1923 PMID: 22388286
- Bullard JH, Purdom E, Hansen KD, Dudoit S. Evaluation of statistical methods for normalization and differential expression in mRNA-Seq experiments. BMC Bioinformatics. 2010; 11:94. https://doi.org/10.1186/1471-2105-11-94 PMID: 20167110